MEASUREMENT OF THE TOTAL CROSS SECTION FOR THE π-2π REACTION p(π^+,$\pi^+\pi^0$)p NEAR THRESHOLD

Nelson Suen

B.A.Sc. University of British Columbia

A THESIS SUBMITTED IN PARTIAL FULFILMENT OF

THE REQUIREMENTS FOR THE DEGREE OF

MASTER OF APPLIED SCIENCE

in

THE FACULTY OF GRADUATE STUDIES

DEPARTMENT OF PHYSICS

We accept this thesis as conforming

to the required standard

THE UNIVERSITY OF BRITISH COLUMBIA

August 1993

In presenting this thesis in partial fulfilment of the requirements for an advanced degree at the University of British Columbia, I agree that the Library shall make it freely available for reference and study. I further agree that permission for extensive copying of this thesis for scholarly purposes may be granted by the head of my department or by his or her representatives. It is understood that copying or publication of this thesis for financial gain shall not be allowed without my written permission.

Department of Physics

The University of British Columbia

6224 Agriculture Road

Vancouver, Canada

V6T 1W5

Date: 30 August 1993

Abstract

A feasibility study for measuring the total cross section of the π-2π reaction, $\pi^+p \rightarrow \pi^+\pi^0p$, was performed at incident pion kinetic energies of 195 and 201 MeV. It was not possible to measure the total cross section with the present apparatus. Modifications and improvements to the present apparatus are presented.

Table of Contents

List of Tables

List of Figures

Acknowledgements

First and foremost, I would like to thank Dr. Richard Johnson for supervising and supporting this work. His insights, experience and humour have been invaluable in the completion of this work. I would also like to thank Dr. Ami Altman for his assistance in so many areas and his excellent explanations for so many of my questions. Special thanks must be given to Dr. Eli Friedman for his PH3J5 program for performing the Monte Carlo simulation and his readiness in sharing his knowledge; and also to Dr. David Axen for reading this thesis. Finally, I would like to thank my old friend Patrick for his good advice and encouragement.

Dedication

To the Rose of Sharon

Chapter 1

Introduction

1.1 Motivation for the Experiment

The motivation for performing this experiment has its roots in the study of the strong interaction, in the low energy regime. Early theoretical work in the field have been based on the idea of chiral symmetry[1] breaking. Contemporary treatment of the subject in terms of quantum chromodynamics (QCD) still relies on the idea of chiral symmetry which is the only rigorous formalism of QCD at low energies.

Traditionally, the test of the validity of various theories that make use of chiral symmetry breaking takes place in trying to measure physical quantities associated with the reaction $\pi^{\alpha} + \pi^{\beta} \rightarrow \pi^{\gamma} + \pi^{\delta}$ (π-π scattering), perhaps the most fundamental of all hadronic processes[2]. Because of the short lifetimes of the pions, π-π scattering cannot be observed directly. Instead, one resorts to indirect means: one such method involves the measurement of cross sections for the π-2π reactions. Cross sections for these reactions

---

[1] Chiral symmetry in this case refers to the symmetry that exists if quarks were massless. In terms of quark theory, the QCD Lagrangian in the chiral limit would consist of two separate parts: one for right-handed particles another for left-handed particle with no coupling between the two. Hence, in the massless quark limit, the left-handed states do not mix with the right-handed states. In the real world, chiral symmetry is not preserved since quarks are not massless.

[2] 'most fundamental of all hadronic process' because π-π reactions involve the self-interaction of the lightest particle in the hadron spectrum of particles.

near threshold can be used to calculate π-π scattering quantities (Fig. 1.2). Early work [15,16] in the field suggested the behaviour of π-π interactions is embodied in a single theoretical parameter[3] ξ; other physical quantities such as scattering lengths are given in terms of ξ. Contemporary theory based on QCD such as chiral perturbation theory makes somewhat different predictions from those of earlier theory. It is the intent of the current experiment to test the predictions of existing theory by measuring the cross section of a π-2π reaction. For a survey of measurements of different π-2π channels and the theoretical description of chiral symmetry breaking refer to [3,23].

1.2 World Data on Reaction

For the π-2π reaction, $\pi^+ p \rightarrow \pi^+ \pi^0 p$, very few measurements have been performed to date: indeed no measurements exists near the threshold energy ($T_{\pi+} = 164.75$ MeV).

$T_{\pi+}$(MeV)	$\sigma(\mu b)$	Reference
230 ± 13	$18 \pm ^{12}_{9}$	[10] (1975)
275 ± 15	$48 \pm ^{34}_{25}$	[10] (1975)
294 ± 4	120 ± 50	[11] (1972)
$300 \pm ?$	110 ± 40	[30] (1963)

Table 1.1 World data on the $\pi^+ p \rightarrow \pi^+ \pi^0 p$ channel (reproduced from [2]).

[3] Known as the 'chiral symmetry breaking' parameter.

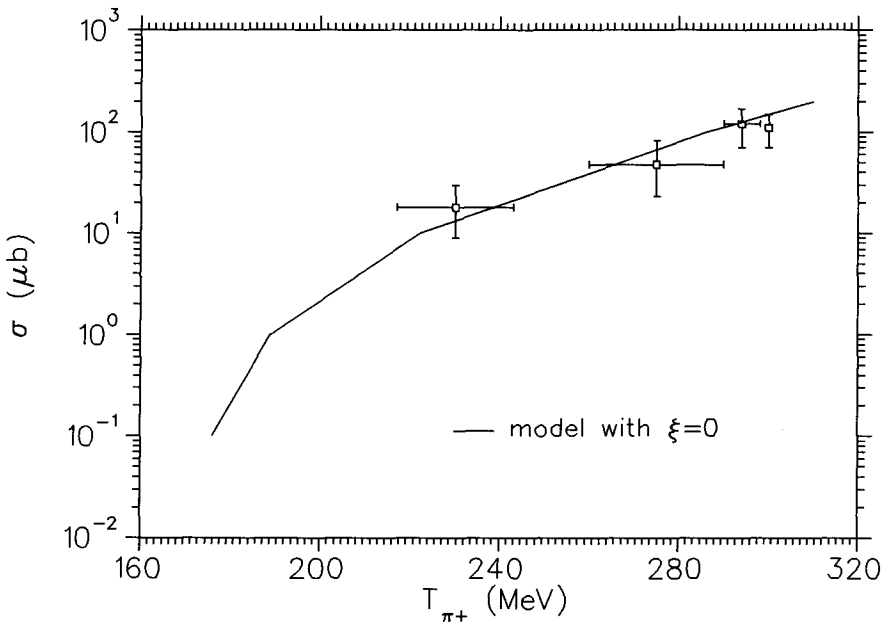

Figure 1.1 World data for the π^+ p → π^+ π^0 p channel (reproduced from [2]). The Oset and Vicente-Vacas model was used to generate the curve for the total cross section.

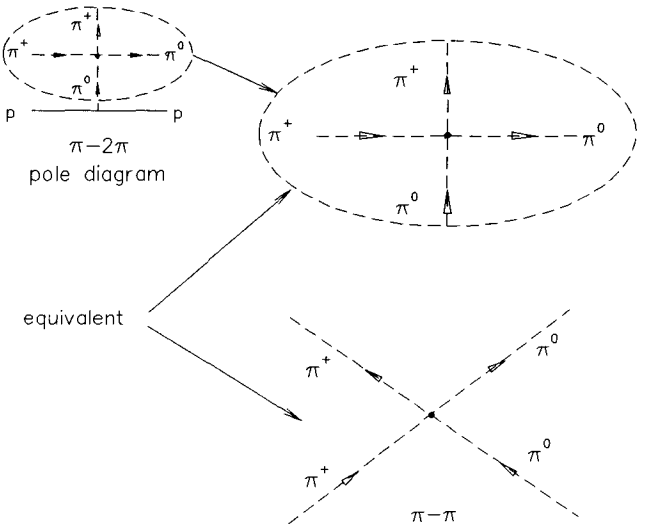

Figure 1.2 Feynman diagrams showing π-π scattering imbedded in π-2π scattering.

It is not at all surprising the data is sparse since, as we shall see, the measurement of the cross section for this reaction is a challenging undertaking, due to the host of background reactions.

1.3 A Semi-Historical Survey of Chiral Symmetry

1.3.1 Weinberg and Schwinger

The first work on chiral symmetry was performed by Steven Weinberg during the early 1960's. Weinberg introduced chiral symmetry breaking to current algebra and the partial conserved axial current (PCAC) hypothesis[4], in order to calculate the π-π scattering lengths[5]. Based on this approach, Weinberg also developed a Lagrangian for the π-π interaction [13]. At about the same time, Schwinger, using a different approach arrived at a different π-π Lagrangian [14].

---

[4] the notion of a partially conserved axial current originates from the idea allowing the quarks to have a small mass (a few MeV's) and therefore breaking the chiral symmetry. It can be shown that the preservation of chiral symmetry implies the conservation of the axial current. To slightly break the symmetry with small quark masses implies that the axial current is partially preserved.

[5] the scattering is defined as

$$\frac{1}{4\pi}\lim_{\lambda\to\infty}\sigma = a^2$$

where a is the scattering length and λ is the wavelength associated with the incident particle.

1.3.2 Olsson and Turner: generalization of the π-π Lagrangian derived by Weinberg and Schwinger.

During the late 1960's Olsson and Turner [15] constructed the most general form of the π-π Lagrangian, which can be considered as a family of Lagrangians because it contains a single free parameter ξ. According to this model, at low energies, ξ the chiral symmetry breaking parameter alone determines the strength of the π-π interaction at low energies. Furthermore, the Weinberg and Schwinger Lagrangians are two specific cases of the Olsson-Turner family of Lagrangians corresponding to the ξ values of 0 and 1, respectively.

1.3.3 Oset and Vicente-Vacas

The model constructed by Oset and Vicente-Vacas for π-2π reactions, adds to the Olsson and Turner model the effects of the intermediate isobar states of the N^* and Δ [22].

1.3.4 Current Theory

One obvious short coming of the Olsson-Turner model is that it does not include π-π rescattering effects. Modern theories that include rescattering effects make significantly different predictions on the scattering lengths. One such approach based on QCD is chiral perturbation theory (ChPT) [17,23,27]. Predictions made by ChPT for the $\pi^+p \rightarrow \pi^+\pi^0p$ reaction will be discussed below.

1.4 Predictions of the Olsson-Turner Model

In the framework of chiral symmetry, the Olsson-Turner Model makes specific predictions that can be experimentally verified. Specifically, we wish to investigate the nature of chiral symmetry breaking by studying π-π scattering amplitudes at zero relative momentum. Because of the short lifetimes of the π, measurement of the amplitudes must be done indirectly. One such method is to measure the cross sections of the $\pi N \rightarrow \pi\pi N$ (π-2π) reactions, near threshold [15].

According to Olsson and Turner's model, the total cross section at threshold for the π-2π reactions is given by [10,16,20]

$$\sigma(\pi N \rightarrow \pi\pi N) = a(\pi\pi N)^2 Q^2 S \times (phasespace) \tag{1.1}$$

For the reaction $\pi^+ p \rightarrow \pi^+\pi^0 p$, the total cross section becomes

$$\sigma = a(\pi^+\pi^0 p)^2 Q^2 \times (phasespace) \tag{1.2}$$

where Q = momentum of incident π^+ in the center of mass system

$a(\pi^0\pi^+ p)$ = the reaction amplitude at threshold, dimensionless in this notation

S = statistical factor accounting for pions in the final state; S = ½ if final pions are identical; S = 1 otherwise.

The threshold amplitude is related to the chiral symmetry breaking parameter ξ in the following way [15,19]

$$2\sqrt{2}a(\pi^+\pi^0 p)=1.51+0.6\xi \tag{1.3}$$

Furthermore, the s-wave π-π scattering lengths[6] for isospin I=0 and I=2 are given by

$$\frac{a_2}{a_0}=\frac{\xi+2}{\frac{5}{2}\xi-7} \tag{1.4}$$

and

$$2a_0-5a_2=\frac{3m_\pi}{4\pi f_\pi^2} \tag{1.5}$$

where f_π = the pion decay constant

m_π = pion mass

---

[6] Because the spin (intrinsic angular momentum) of the pion is zero and at threshold the angular momentum l=0, only s-waves are present.

Symmetric wave function (boson symmetry) under the interchange of pions of a π-π system further dictates that the isospin be even. Therefore for the π-π system at threshold, I=1 isospin components vanish leaving only I=0,2 components [3]. In terms of the scattering lengths a_I only a_0 and a_2 remains.

Combining (1.4) and (1.5) yields and using f_π=93.3 MeV

$$a_0=(0.156-0.0560\xi)m_\pi^{-1} \tag{1.6}$$

$$a_2=-(0.045+0.0224\xi)m_\pi^{-1} \tag{1.7}$$

In summary, according to the Olsson-Turner model, by measuring the total cross section σ, the threshold amplitude a($\pi^+\pi^0$p) can be determined using (1.2). It follows that by (1.3) allows ξ is determined and by (1.6),(1.7) the scattering lengths are found. Table 1.2 gives the values for the scattering lengths for $\xi=0$.

	a_0	a_2
Weinberg [18] (Olsson-Turner $\xi=0$)	0.16	0.045
Gasser & Leutwyler [17] (Chiral Perturbation Theory)	0.20	-0.042

Table 1.2 Scattering lengths predictions from different theoretical models. a_I are in units of $(m_\pi)^{-1}$, where I is Isospin.

1.5 Chiral Perturbation Theory

Gasser and Leutwyler [24] have made predictions on the π-π scattering lengths using ChPt (see Tab. 1.2). Based on Gasser and Leutwyler's work, Donoghue [28] has calculated the π-π chiral scattering amplitudes. ChPt makes use of chiral effective Lagrangians [27], which are classified according to expansion in terms of energy. The lowest order Lagrangian is of the order E^2 (energy squared). At this order, the π-π Feynman diagrams are at 'tree-level'

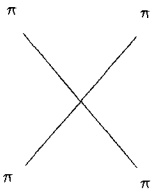

Figure 1.3 Tree level diagram.

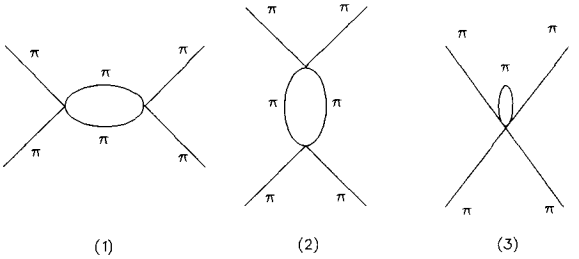

Figure 1.4 Loop level diagrams which contribute to scattering amplitudes.

(Fig. 1.3); that is, no rescattering effects are considered.

The predictions made at this order reproduces the scattering lengths proposed by Weinberg [1] (which corresponds to the Olsson-Turner model with $\xi = 0$). The Lagrangian at order E^4 has been calculated by Gasser and Leutwyler [27]. At this order, calculations involve one-loop diagrams (Fig. 1.4). Imbedded in the Lagrangian to order E^4 are two 'free parameters' $\tilde{\alpha}_1$ and $\tilde{\alpha}_2$ which are to determined by experiment.

In what follows, the π-π scattering amplitudes (see [28]) derived by Donoghue will be used in conjunction with the intermediate isobars Δ and N^* portion of the Oset and Vacas-Vicente model to generated cross sections for the different π-2π channels. The following calculations will follow the approach by V. Sossi [29]. Figures 1.3 and 1.4 show the cross section generated by this approach. The solid curves for the total cross section are determined by setting the parameters of the Lagrangian to values derived in ref. [28]

$$\tilde{\alpha}_1 = -0.007 \text{ and } \tilde{\alpha}_2 = +0.013$$

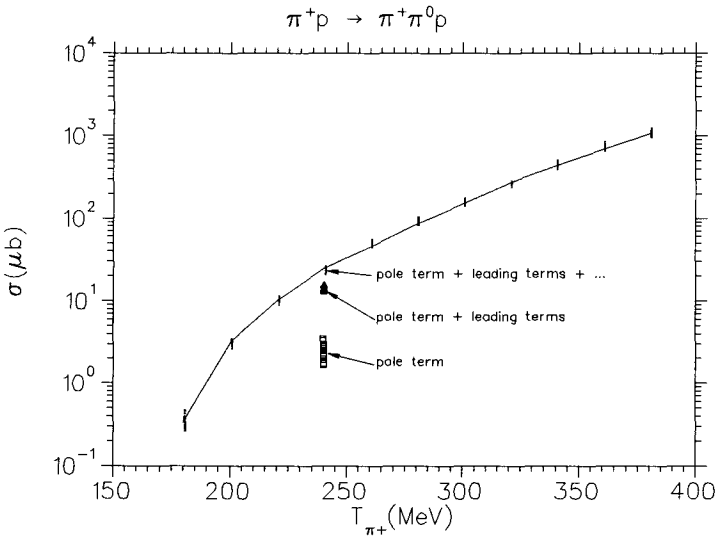

Figure 1.5 Total cross section based on the Donoghue (ChPt) scattering amplitudes along with isobars described by the Oset and Vacas-Vicente model. The solid curve is determined by setting $\tilde{\alpha}_1 = -0.007$ and $\tilde{\alpha}_2 = +0.013$. And the vertical dash marks represent points calculated by varying $\tilde{\alpha}_1 \pm 100\%$ and $\tilde{\alpha}_2 \pm 50\%$.

To determine the sensitivity of the cross section to the parameters $\tilde{\alpha}_1$ and $\tilde{\alpha}_2$, calculations were performed by varying the parameters by 100% and 50% respectively (these points are shown as vertical dash marks in Fig. 1.3 and 1.4). The $\pi^+\pi^+$ channel is included here for comparison as will be discussed.

1.5.1 Feynman Diagrams

Figure 1.7 depicts the Feynman diagrams for the $\pi^+p \rightarrow \pi^+\pi^0p$ reaction. The diagram of primary interest is the pole (1), for studying π-π scattering (see Fig. 1.2). The set of 3-point

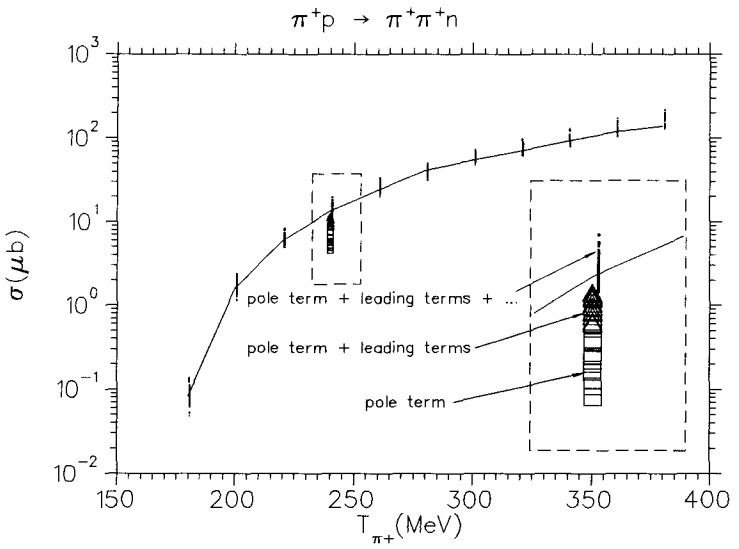

Figure 1.6 Total cross section (see caption on Fig. 1.2).

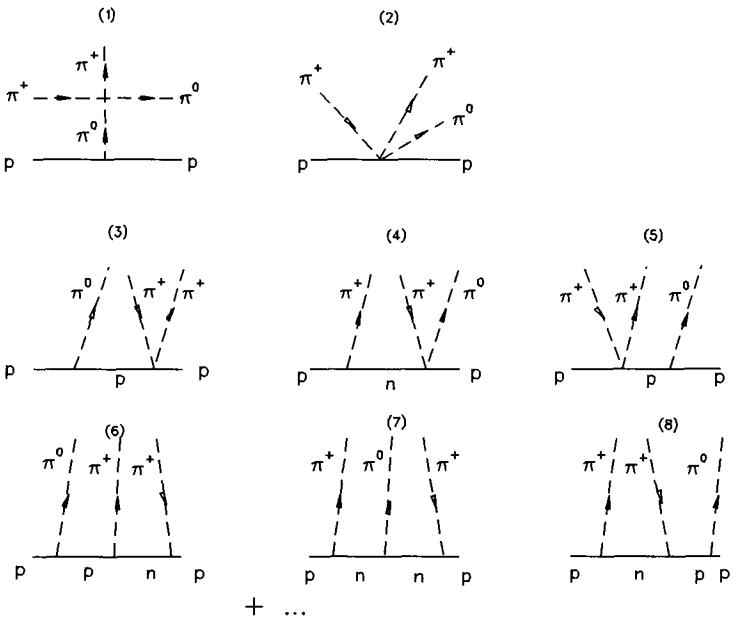

Figure 1.7 Feynman diagrams for the $\pi^+\pi^0$ reaction channel. Note: 3-point diagrams involving isobars are not depicted. Diagrams (2)-(8) are called in this paper the 'leading diagrams' for this channel.

diagrams (6)-(8) in Fig. 1.7 are incomplete, as only nucleon states have been shown. There are 22 other 3-point diagrams containing a mix of (nucleon-Δ), (nucleon-Δ-Δ) and (nucleon-Δ-N^*) states (see ref. [3] for more diagrams). All diagrams contribute to the total cross section and are used to determine the total cross section. For this channel, the pole term accounts for 30% of the total cross section at $T_{\pi+}$=180 MeV and less at higher energies (Table 1.3). Even at modest energies, isobar states begins to dominate causing the pole term contribution to diminish to 10% at 240 MeV (Fig. 1.9).

$T_{\pi+}$(MeV)	180	240
% of total cross section σ		
pole diagram	30	10
leading diagrams (see Fig. 1.7)	48	44
isobars and nucleons diagrams	22	46

Table 1.3 Proportion of contributions to the total cross section for different diagrams for the $\pi^+\pi^0$ channel.

$T_{\pi+}$(MeV)	180	240
% of total cross section σ		
pole diagram	88	45
leading diagrams (see Fig. 1.8)	1	37
isobars and nucleons diagrams	11	18

Table 1.4 Proportion of contributions to the total cross section for different diagrams for the $\pi^+\pi^+$ channel.

Figure 1.8 depicts the Feynman diagrams for the $\pi^+p \rightarrow \pi^+\pi^+n$ reaction. Again, the set of 3-point diagrams are incomplete, as only nucleon states have been included. But overall there are far less number of diagrams for this channel especially those that involve the

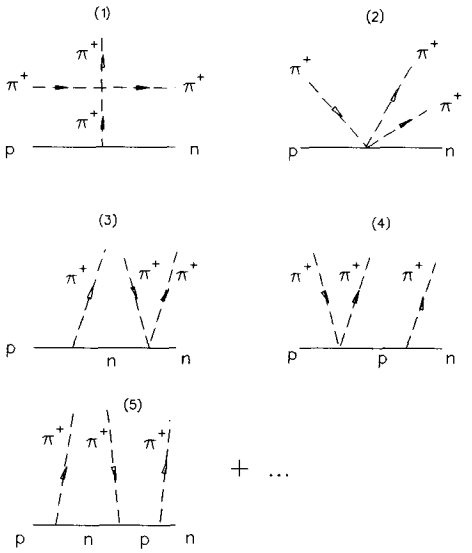

Figure 1.8 Feynman diagrams for the $\pi^+\pi^+$ channel. Note: 3-point diagrams involving isobars are not depicted. Diagrams (2)-(5) are called in this paper the 'leading diagrams' for this channel.

isobar states. There are only 11 other 3-point diagrams containing a mix of (nucleon-Δ), (nucleon-Δ-Δ) and (nucleon-Δ-N*) states (see ref. [3] for more diagrams), in contrast to the 22 for the $\pi^+\pi^0$ channel. Further, in sharp contrast, for this channel, the pole term accounts for 88% of the total cross section at $T_{\pi+} = 180$ MeV (Table 1.4). Isobar states play much less of a role for this channel whose contribution to the total cross section increases from 11% to 18% between 180 MeV and 240 MeV (Fig. 1.10).

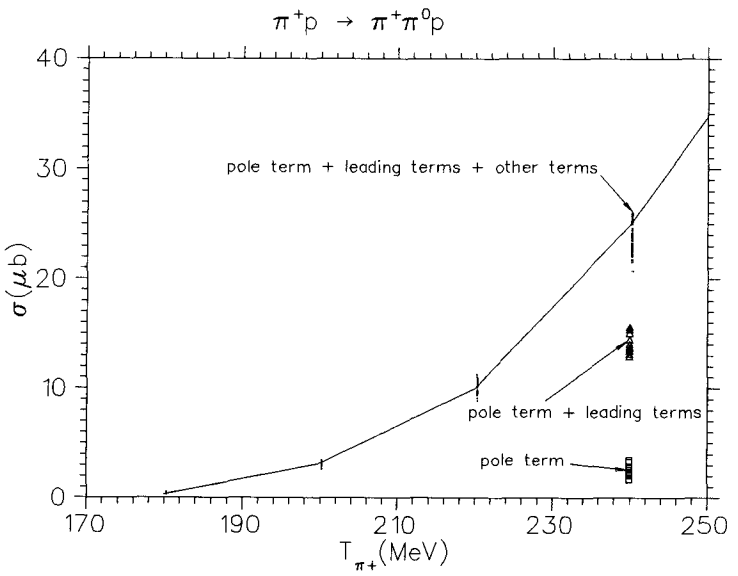

Figure 1.9 Different contributions to the total cross section.

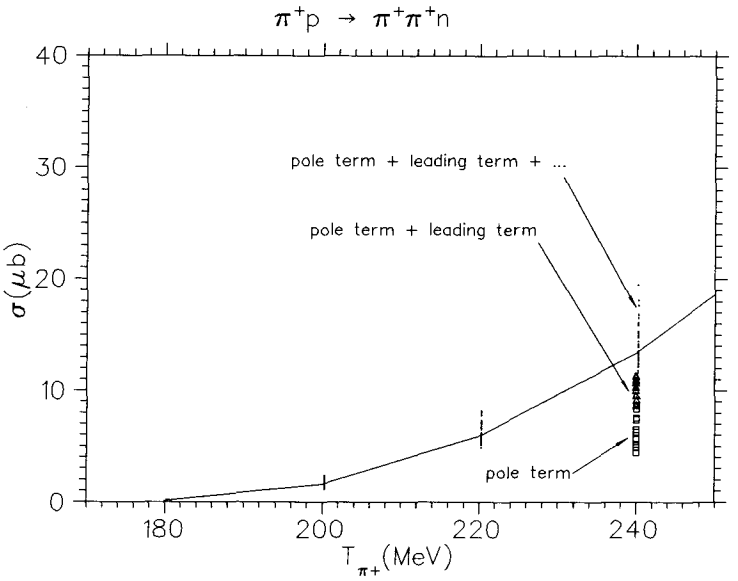

Figure 1.10 Different contributions to the total cross section.

1.5.2 Sensitivity of the π-π (Pole) Contribution

As mentioned above, the pole diagram accounts for only a fraction of the total cross section; since the physics of π-π scattering is imbedded in the pole term the magnitude of its contribution to the total cross section is determined by the parameters $\tilde{\alpha}_1$ and $\tilde{\alpha}_2$. As shown in Figs. 1.5 and 1.6, by varying the these parameters and looking at the changes in total cross section one can determine the sensitivity of the pole term.

It will be shown below that the $\pi^+\pi^0$ channel is 'insensitive' to changes in $\tilde{\alpha}_1$ and $\tilde{\alpha}_2$ in the region near threshold (say, from threshold up to 320 MeV). By 'insensitive', two things are implied: first, the variation in cross section is small relative to other channels such as the $\pi^+\pi^+$ and second, perhaps the most important reason, the variation is small relative to existing experimental error levels[7].

For Figures 1.11 and 1.12, the phase space dependence of the total cross section σ has been divided out. It is evident that for the $\pi^+\pi^0$ channel that the variation in cross section is far smaller than errors on existing data points. For this reason, it is not possible to extract useful information about the $\tilde{\alpha}_1$ and $\tilde{\alpha}_2$ parameters, without improving on the previous experimental error levels which are typically $\pm 50\%$ of σ. To pin down the alpha parameters errors should be reduced to $\sim \pm 10\%$ of σ. In contrast, the variation for the $\pi^+\pi^+$ channel is larger or comparable to errors on existing data points.

[7] i.e., the size of the experimental errors on existing experimental data.

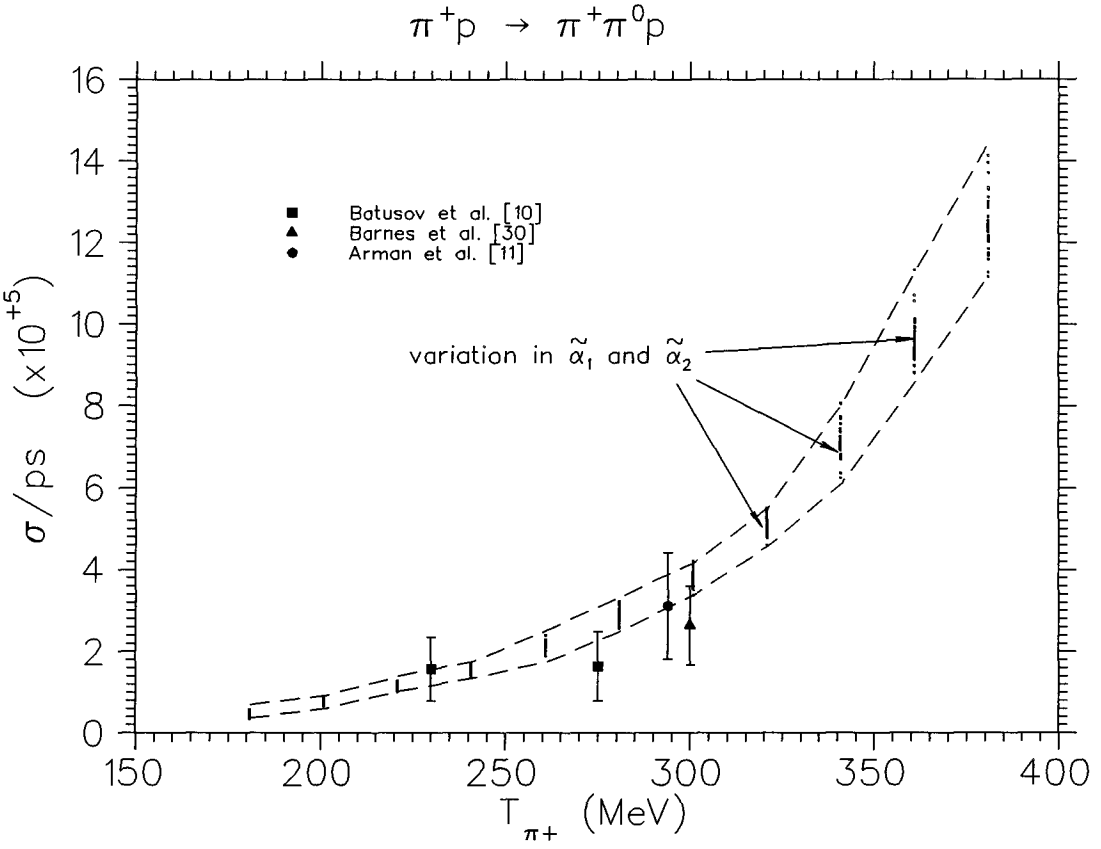

Figure 1.11 $\pi^+\pi^0$ channel, total cross section divided by phase space (dimensionless). The vertical dash marks represent points calculated by varying $\tilde{\alpha}_1 \pm 100\%$ and $\tilde{\alpha}_2 \pm 50\%$ (from the base values of $\tilde{\alpha}_1 = -0.007$ and $\tilde{\alpha}_2 = +0.013$), while the broken line outlines the region mapped out by this variation.

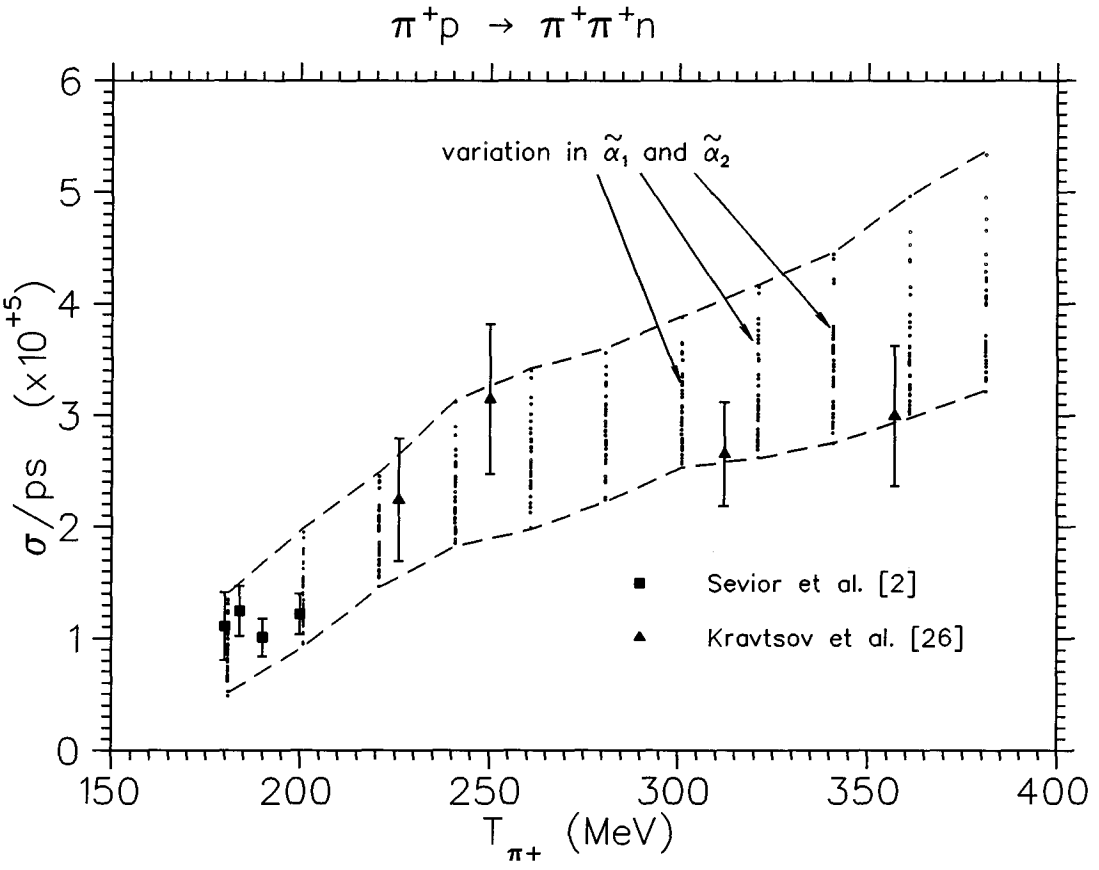

Figure 1.12 $\pi^+\pi^+$ channel, total cross section divided by phase space (dimensionless). The vertical dash marks represent points calculated by varying $\tilde{\alpha}_1 \pm 100\%$ and $\tilde{\alpha}_2 \pm 50\%$ (from the base values of $\tilde{\alpha}_1 = -0.007$ and $\tilde{\alpha}_2 = +0.013$), while the broken line outlines the region mapped out by this variation.

Recent measurements by Sevior et al. [2] near threshold contain errors which are small enough to constrain the alpha parameters. The errors for the Sevior experiment are typically $\sim 20\%$ of the total cross section, which are less stringent than the 10% requirement for the $\pi^+\pi^0$ channel. Figure 1.13 show the fractional change in the total cross section as a result of varying the alpha parameters: it is immediately evident that the $\pi^+\pi^0$ channel cross section is far less sensitive to such variation. Figures. 1.14 and 1.15 show the experimental error levels for existing data.

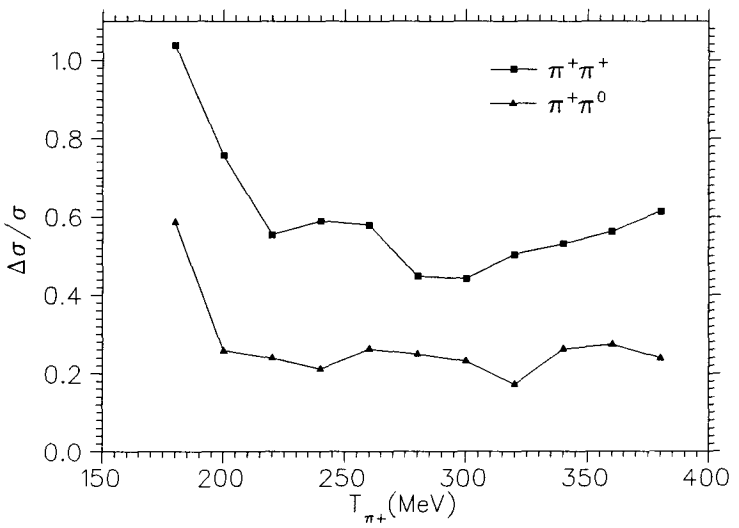

Figure 1.13 Fractional change in the total cross section as a result of variation in the alpha parameters, for the $\pi^+\pi^0$ and $\pi^+\pi^+$ channels.

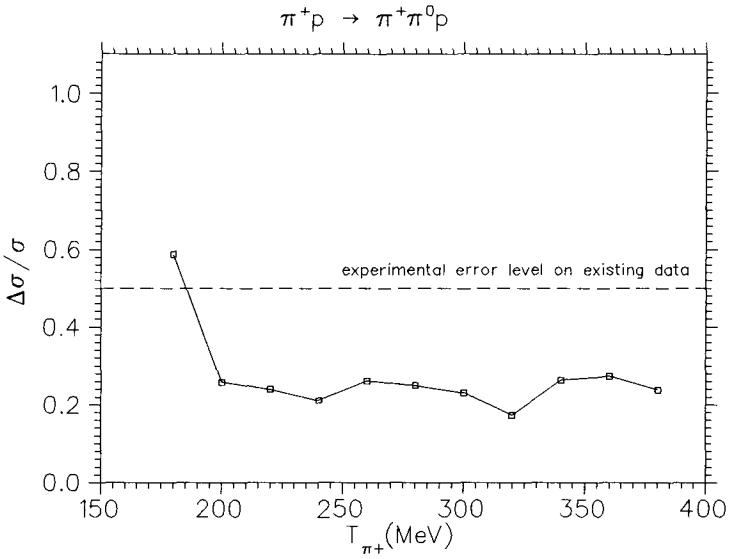

Figure 1.14 Fractional change in the total cross section compared against existing experimental error levels.

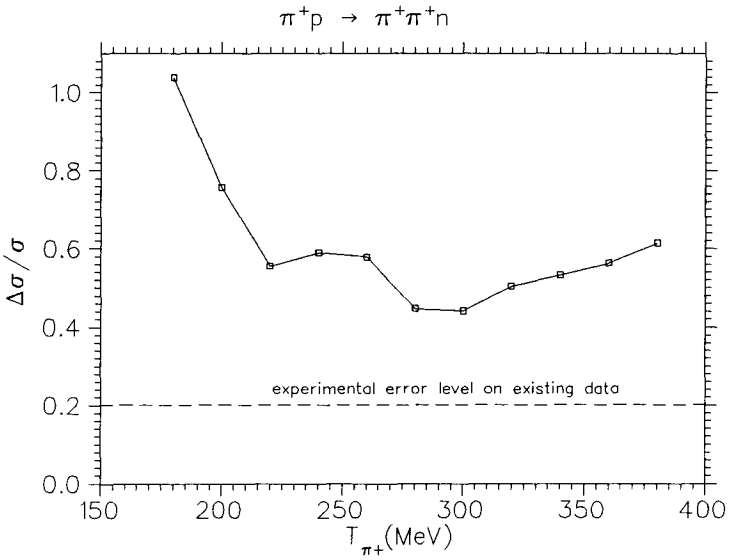

Figure 1.15 Fractional change in the total cross section compared against existing experimental error levels.

If one defines the quantity $\Sigma=\sigma/ps$, where σ is the total cross section and ps is the phase space, then another approach is to consider the ratio of Σ's for the two channels: $\Sigma(\pi^+\pi^+)/\Sigma(\pi^+\pi^0)$. Figure 1.16 shows the plot of this ratio, again with same variation in the alpha parameters as previous defined (see Fig. 1.11). In contrast to Figures 1.11 and 1.12, which shows a small cross sectional variations at energies near threshold and then progressively larger variations at higher energies, the ratio displays a large changes near threshold with progressively small changes at higher energies. While constraining the alpha parameters still require the experimental errors to be smaller than 20% and 10% for the $\pi^+\pi^+$ and $\pi^+\pi^0$ repectively, this approach offers a different perspective in analyzing the cross section data. Figure 1.17 shows changes in the Σ ratio due to the variation in the alpha parameters as well as a $\pm$20% change in the Δ coupling constant. It is clear that for the ratio, changes due to the alpha parameters dominates when compared to those arising from the Δ coupling constant.

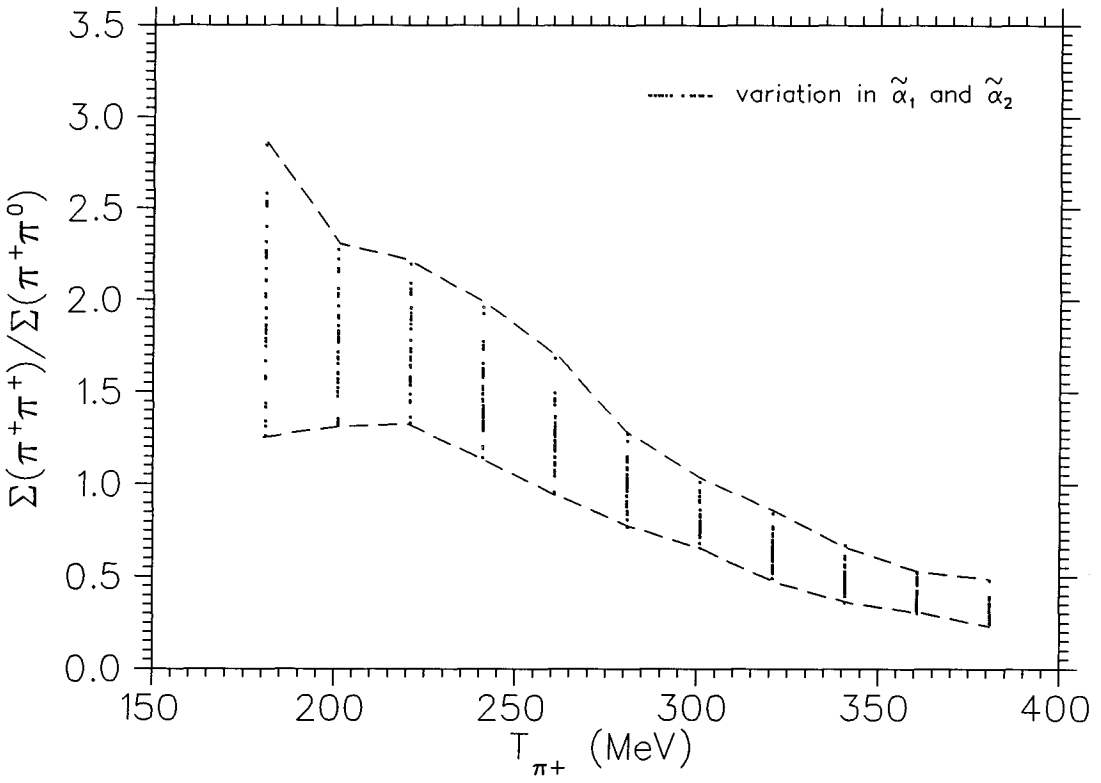

Figure 1.16 The ratio of Σ's for the two channels: $\Sigma(\pi^+\pi^+)/\Sigma(\pi^+\pi^0)$, with same variation in the alpha parameters as previous defined (see Fig. 1.11)

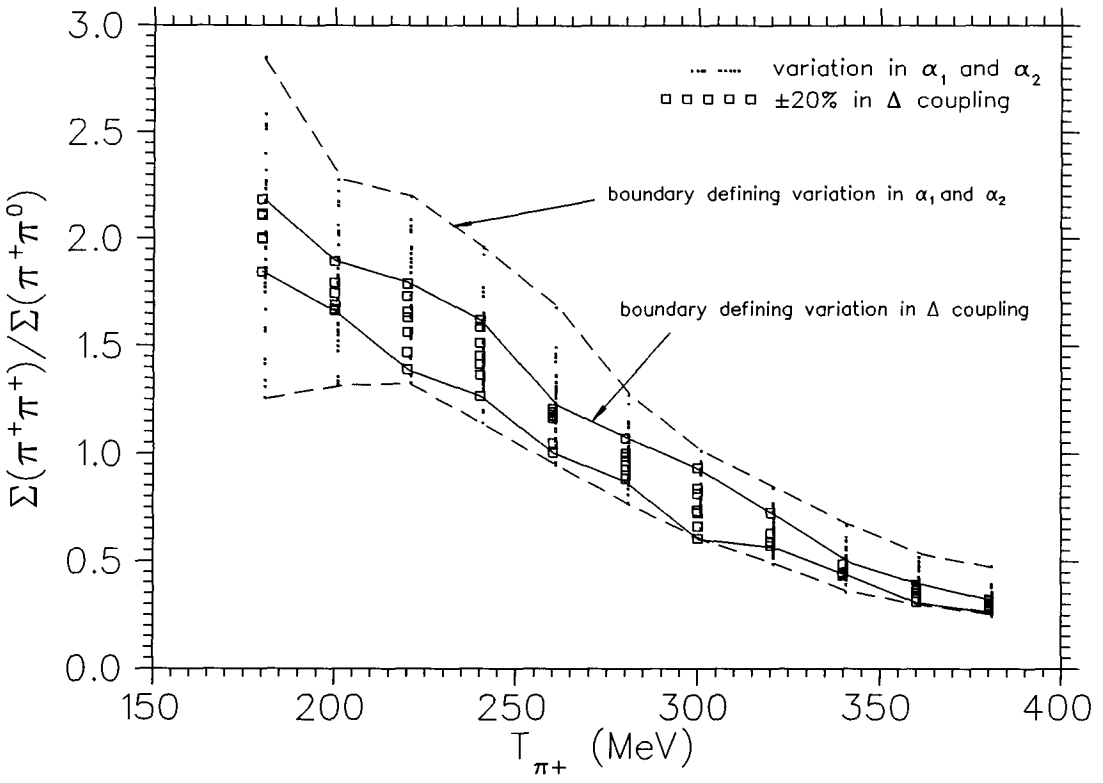

Figure 1.17 Changes in the Σ ratio due to the variation in the alpha parameters as well as a ±20% change in the Δ coupling constant.

Chapter 2

Description of Experiment

2.1 Introduction

This chapter will address how one measures the cross section of reaction (2.1). The experimental apparatus and the technique for eliminating the background events will be introduced.

2.2 General Approach

The purpose of the present experiment is to measure the total cross section for the reaction[1]

$$\pi^+ p \rightarrow \pi^+ + \pi^0 + p \qquad (2.1)$$

near threshold energy of π^0 production (164.75 MeV). At a first glance, this measurement appears relatively simple. However upon closer inspection one finds that there are a number of other reactions occurring at the same time. Therefore, the difficulty in the measurement is to separate the events arising the principal reaction from those of the background reactions. The first category of background reactions arises from other π^+p channels (reactions (2.2)-(2.4)).

[1] Henceforth in this paper, reaction (2.1) will also be referred to as the 'principal' reaction. Of course, this convention is only a necessary prejudice of this paper.

The second category (reaction (2.5)) arises from π^+ collisions with neutrons which are present together with the protons in the solid the C and CH_2 targets.

Ignoring the background reactions for a moment, the technique that can be used to measure the total cross section is to take advantage of the small angles[2] (Fig. 2.1) of the outgoing protons near threshold. For example, for beam pions with kinetic energy of $T_{\pi+}$=220 MeV, the reaction protons are confined within a cone of $(\theta_p)_{max}=36^0$ [3]. The angles are smaller for lower $T_{\pi+}$, with $(\theta_p)_{max}\sim 7^0$ at threshold. Hence, if there were no competing reactions, one can account for all events by simply detecting the outgoing protons within the cone. Before going on to discuss how to distinguish background events from those of the principal reaction, it is necessary to introduce the experimental set-up.

2.3 Details of Set-up

Targets

The targets used in the experiment are solid carbon (C) and polyethylene (CH_2). Due to the low energy of the reaction protons and

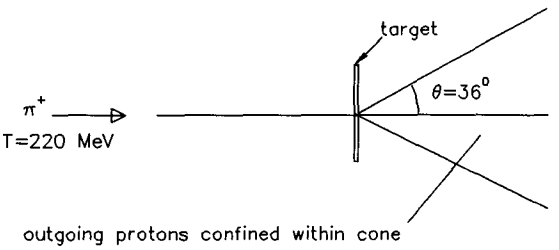

Figure 2.1 Confinement of protons to small cone angles.

[2] i.e., angle of the proton with the beam axis

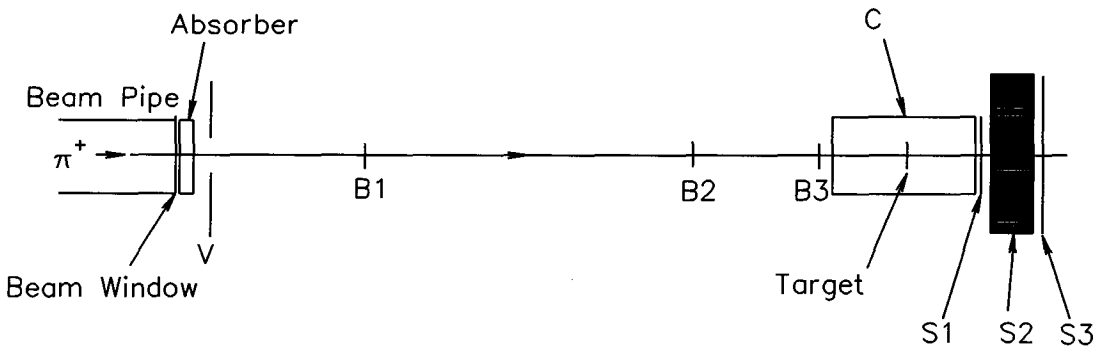

Figure 2.2 Experimental Set-up

$$\pi^+ p \rightarrow \pi^+ + p \tag{2.2}$$

$$\pi^+ p \rightarrow \pi^+ + \gamma + p \tag{2.3}$$

$$\pi^+ p \rightarrow \pi^+ + \pi^+ + n \tag{2.4}$$

$$\pi^+ n \rightarrow \pi^+ + \pi^- + p \tag{2.5}$$

pions, it is necessary to use very thin targets[3] (~ 0.2 g/cm^2). The reason that 2 different

[3] A CH_2 target with thickness of 0.5 g/cm^2, will stop protons with kinetic energy up to 22 MeV and pions up to 9 MeV.

targets are used are as follows. Since we are only interested in the events arising from π^+H_2 (i.e. π^+p) collisions with the CH_2 target, some method must be introduced to remove the unwanted events from π^+C collisions. The way to achieve this is to make 2 separate measurements: one with a CH_2 target and an other with a C target. The results from the 2 measurements are then subtracted (CH_2 events - C events). Subtracting the C events from the CH_2 events effectively removes the events from scattering off carbon leaving only the events from scattering off the 2 protons. This method has already been successfully implemented in measurement of the total cross section of the single charge exchange (SCX) reaction $\pi^-p \rightarrow \pi^0n$ [7,8]. A more detail treatment of this subtraction method is discussed in [5,6].

The Proton Absorber

An aborber made of polyethylene (CH_2) with thickness 1.9 g/cm^2 is placed in front of the beam window to remove protons that have 'leaked' through with the beam pions.

Beam Defining Counters

Four scintillator counters (NE102) V, B1, B2 and B3 are used for beam definition. An incident beam pion accepted is defined[4] as the coincidence of B's anticoincidence with V. The purpose of the V or 'halo' counter is to eliminate any stray (outside the main beam)

[4] i.e., in boolean algebra B1 AND B2 AND B3 AND (NOT V).

particles that causes a coincidence in the B counters (see Appendix A and C).

The Event Detectors

Events are defined by a group of 4 detectors, also NE102 scintillators: C, S1, S2 and S3. The S1 and S2 detectors make up the 'telescope' array which is the heart of the experiment for looking at reaction events. The principle of how this telescope works will be discussed in detail below. The rest of the detectors C and S3 are used to reject unwanted background events. The C or 'cylindrical' detector is used to reject events from background reaction (2.5). The S3 veto detector is used to eliminate events from background reactions with high energy particles that manage to traverse the entire array of detectors and target, 'coming out the other side'. These particles mainly arise from elastic scattering and beam particles that did not interact[5] with the target. An 'event' is defined[6] as the coincidence of S1 and S2, anticoincidence with C and anticoincidence with S3 (see Appendix A and C).

The S1-S2 Telescope Array

A single scintillator detector by itself cannot identify what type of particle has traversed it. To see why this is the case, we first investigate what happens to a charged particle travelling through a medium. For a charged particle whose mass is much greater than the mass of the

[5] i.e., the strong interaction.

[6] In boolean form, an 'event' is (S1 AND S2) AND (NOT C) AND (NOT S3).

electron, energy loss in traversing a medium is due primarily to the interaction of the particle with the atomic electrons in the medium. The mean rate of energy loss due to the ionization of electrons is given by the Bethe-Bloch formula[7] is given by

$$\frac{dE}{dx} = \frac{4\pi N z^2 e^4 Z}{m_e \beta^2 c^2}\left[\ln\left(\frac{2m_e\beta^2c^2}{I(1-\beta^2)}\right) - \beta^2\right] \tag{2.6}$$

where
m_e = electron mass
z = charge (in units of e) of traversing particle
$\beta = v/c$
v = velocity of traversing particle
Z = atomic number of atoms in medium
N = number density of atoms in medium

x = path length in medium
I = an effective ionization potential, averaged over all electrons $\sim 10Z$ eV

Suppose that we have a very thin[8] medium (S1) with width dx, then knowing all the medium parameters, one can extract the velocity of the traversing particle by measuring dE. There is no way to identify the mass of particle since (2.6) is independent of this mass. The way to identify the particle is to determine its total energy by adding a second thicker medium

[7] A semi-classical derivation of this formula is given in [8]. This equation is the 'basic' Bethe-Bloch formula without any terms for shell corrections or density corrections at higher energies.

[8] The 'thin' assumption is to simplify the argument making the velocity approximately constant through the medium. For a finite δx medium the velocity is through the medium is not constant but one can easily devise an algorithm to extract the velocity upon exit of the medium by dividing the entire medium into smaller pieces and accounting for the velocity difference upon entrance and exit of each little piece of material and proceed then through the entire medium.

(S2) which stops the particle completely. The second medium records an energy deposition E. Hence, the total energy of the traversing particle is E+dE. The mass M of the particle is given by

β in (2.7) given by (2.6).

In practice, one does not calculate the mass explicitely to identify the particle. By plotting

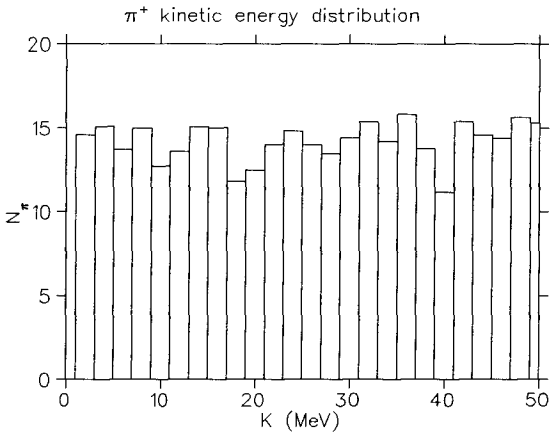

Figure 2.3 A 'uniform' distribution of pions.

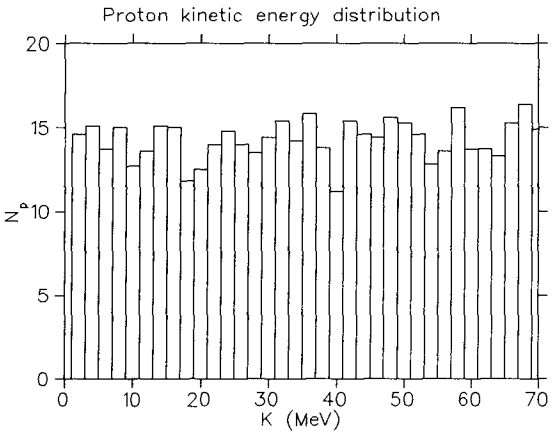

Figure 2.4 A 'uniform' distribution of protons.

the S1 signal versus the S2 signal (i.e., ΔE vs E) one can readily identify a particle. Sending a host of particles with the same mass but different energies through the S1-S2 telescope will trace out a unique 'band' in the ΔE vs E plane. To show this effect, imagine sending a uniform distribution of π^+ with kinetic energy between 0 and 50 MeV (Fig. 2.3) and also

a uniform distribution of protons between 0 and 70 MeV (Fig. 2.4). Figure 2.5 shows the band structure corresponding to each type of particle.

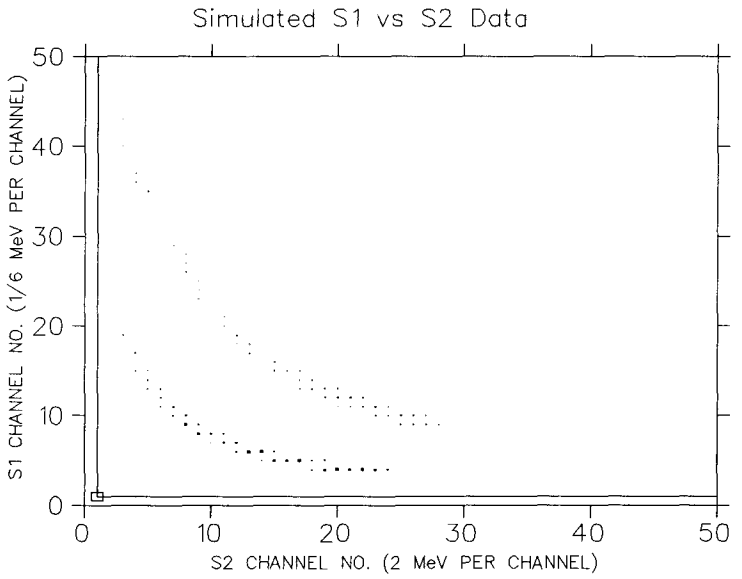

Figure 2.5 The 'band' structure for different masses in the ΔE vs E plane. The top group is the proton band while the bottom is the pion band. Progressively larger massess would trace out bands higher up in the plane.

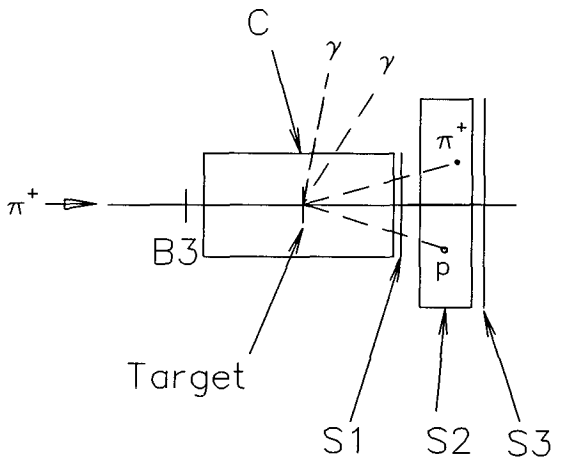

Figure 2.6 Typical 'pile-up' event. The two gamma rays come from the decay of the π^0.

2.4 A Brief Tour of a Reaction Event

With the telescope, we are now ready to look at reaction events. As shown above, one can not only identify whether a pion or proton has struck the S1-S2 array but also the energy of the particle. A beam pion begins upstream and then through the aborber, through the V halo veto, gets accepted by B1 B2 B3 and then reacts with the target. Let us suppose that the principal reaction takes place then what is emitted from the target is a proton, a π^+, and a π^0. The π^0 will escape without being detected[9]. The proton is restricted by phase space to be within a certain angle: all that is needed is to make S1-S2 large enough to cover the cone angle, catching all protons and some of the π^+ with the detector. In this way, with the

[9] In principle, one can detected the π^0 via its decay to 2 gamma rays. In reality due to the high energy of the gamma's (interaction cross section falls off with increasing energy) from the π^0 of this reaction, a very large and expensive detector is needed.

absence of background reactions, the total cross section of the principal reaction is determined.

2.5 Strategy for Eliminating Background Events

To eliminate the background reactions, we need to determine which background events will fall in the acceptance angle of the S1-S2 telescope. Since we can achieve mass and energy resolution with the telescope, if the background events have energies which are radically different than (2.1), then they will appear in a different region of the ΔE vs E plane. So, the general strategy in modelling the background is to send a distribution of particles that belong to the phase space of a particular background reaction and determine their signatures in the ΔE vs E plane.

The result of this analysis (see Chap. 3) is clear, to distinguish events from the reaction of interest and background reactions, one should consider a smaller group of outgoing protons that fall in the kinematical cone: those that strike the S1-S2 detector accompanied by a π^+, (Fig. 2.6) Thus we ignore those protons that hit the telescope without an accompanying pion. The reason for rejecting these protons is that they fall in a region ΔE vs E riddled with background events. However, the signatures of the smaller group of (proton & π^+) or 'pile-up' events are uniquely determined in the ΔE vs E plane, with the only exception of reaction (2.5). This reaction also possesses simultaneous events of the form of either π^+p or π^-p,

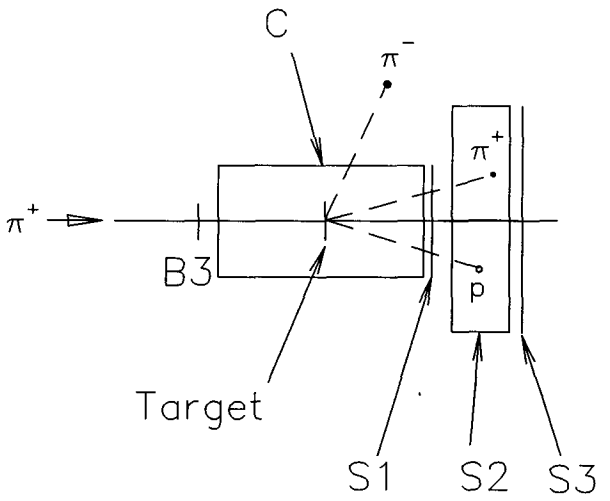

Figure 2.7 Typical event vetoed by the 'C' detector.

which appear in the same region of the ΔE vs E plane. However, this competing reaction is accompanied by an additional charged pion. This difference is used to eliminate the overlap in events: a cylindrical veto counter (C) is introduced to reject simultaneous πp events coincident with another charged π (Fig. 2.7).

As it will be discussed later (see Chapter 5), the use of time-of-flight will be very important in separating another type of background events from those of the principal reaction. These background events are different from those[10] above. In this case the background comes

[10] i.e., reactions (2.2)-(2.5).

from the beam interacting with the 'B' and 'S' detectors. In a very real sense, these detectors are themselves targets, producing a host of events. The trick here is to isolate only those events that are coming from the target: this is where time-of-flight separation is crucial.

To summarize, the elimination of the background events is a 2 stage process: first one

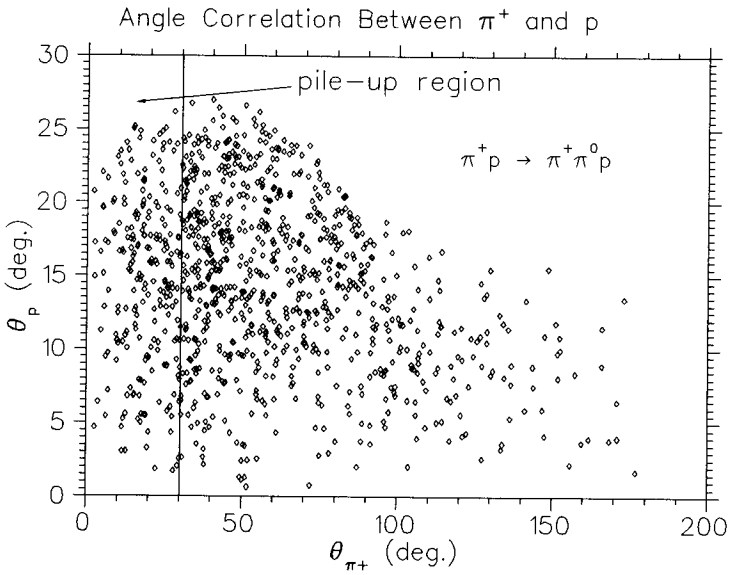

Figure 2.8 Pile-up events are those that appear in the left window.

eliminates the 'detector' background using time-of-flight; second having separated out the target events during the first stage, then one uses the 'pile-up' events to separate 'target' background events from those of the principal reaction.

By restricting the accepted events to pile-up events, one can only measure a fraction of the total cross section of (2.1). This fraction is sometimes referred to as the 'efficiency' η. From phase space considerations alone, the proportion of pile-up events to total events yields $\eta = 0.22$, at an incident pion kinetic energy of 200 MeV. Table 2.1 shows different values of η at different pion kinetic energies, with an acceptance angle corresponding to $(\theta_p)_{max}$, for the first 3 energies and 30^0 for 200.0 MeV.

$T_{\pi+}$ (MeV)	$(\theta_p)_{max}$	$(\theta_{\pi+})_{max}$	η
167.0	7.19^0	40.96^0	0.120
180.0	18.40^0	175.61^0	0.159
190.0	23.28^0	176.55^0	0.184
200.0	26.99^0	176.86^0	0.221

Table 2.1 Maximum angles and η (percent of total cross section measured) from phase space calculations at different energies.

Figure 2.8 shows the correlation between angles of the outgoing π^+'s and protons: the pile-up events appear in the window on the left. Monte carlo simulations that account for non-linearity of light output in the scintillor detectors and a 10% FWHM[11] photoelectron statistics give $\eta \sim 15\%$.

[11] 'Full Width at Half Maximum'. For an explanation of photoelectron statistics as it relatives to energy resolution of scintillator detectors see 'Glenn F. Knoll, *Radiation Detection and Measurement*, John Wiley & Sons (1979), Chapter 10.

2.6 Conclusion

In this chapter, we have described the expermental apparatus; also, the 2 different types of background events were introduced: the first comes from the beam interacting with the detectors while the second comes from background reactions. Different methods for eliminating these background events were introduced. In the next chapter, we will look in detail the technique for eliminating events from background reactions developed from Monte Carlo simulation.

Chapter 3

Modelling of Experiment

3.1 Introduction

In the previous chapter, we discussed the use of 'pile-up' events for measuring the cross section of reaction (2.1). Much of this analysis is based on the Monte Carlo simulation of the experimental set-up. A 'standalone' routine 'PH3J5' was written by Eli Friedman of the Hebrew University Jerusalem to perform this analysis. We will demonstrate how events from reaction (2.1) can be isolated from those of reactions (2.2)-(2.5).

3.2 Phase Space

To gain a better understanding of the difficulty in separating the reaction events from background reaction events, let us consider the phase space of all the reactions.

All the calucations below are performed at a kinetic energy of $T_{\pi+}$=200.0 MeV, for the incident π^+.

For reaction (2.1) $\pi^+ p \rightarrow \pi^+ \pi^0 p$, Figures 3.1-3.3 show the number distributions in the kinetic energy space for each of the particles on the right-hand side of the reaction. An important phase space feature of the reaction is shown in Fig. 3.4, where we see that the outgoing protons are confined to a relatively small angle, $(\theta_p)_{max}=27^0$.

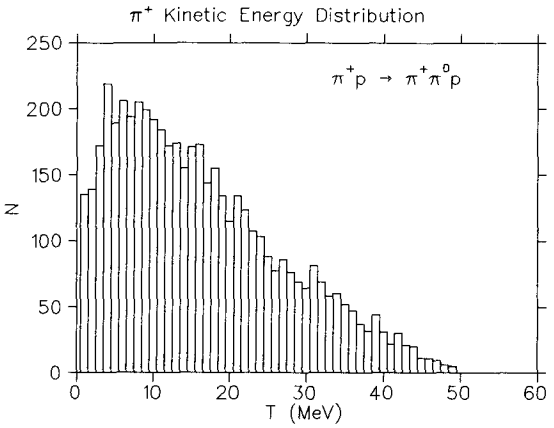

Figure 3.1

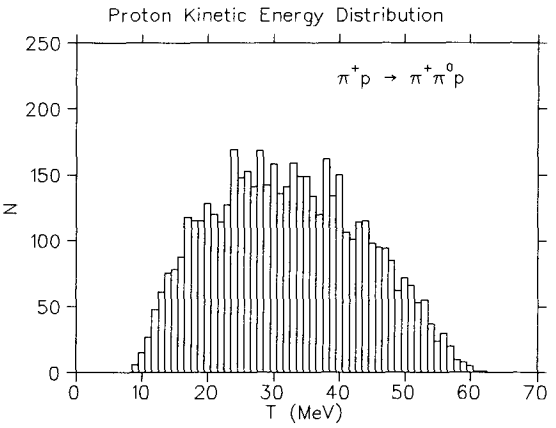

Figure 3.2

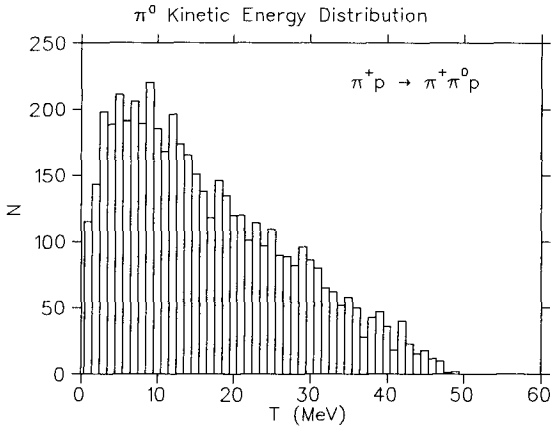

Figure 3.3

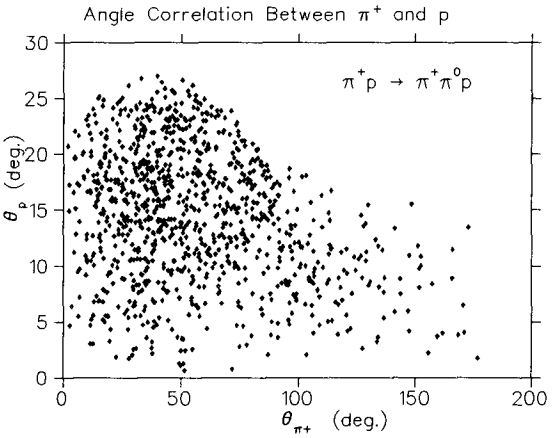

Figure 3.4

For elastic scattering (2.2) $\pi^+p \rightarrow \pi^+p$, Figure 3.5 shows that the kinetic energy range of the outgoing π^+'s do not overlap the range of outgoing π^+'s of (2.1). However, Figure 3.6 shows

the kinetic energy range of the outgoing protons contains the range of the protons from the principal reaction (2.1). It is already evident by including the elasic channel in our analysis that some way must be used to separate the reaction events from background events.

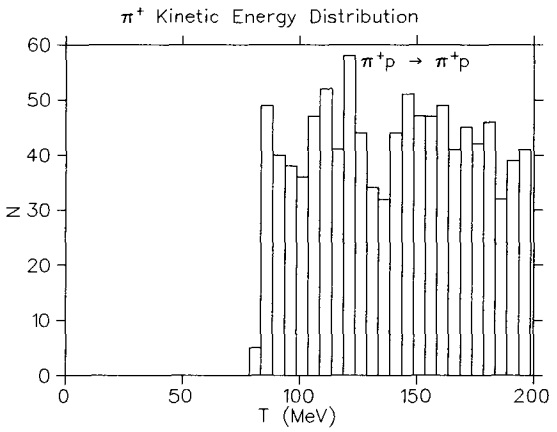

Figure 3.5

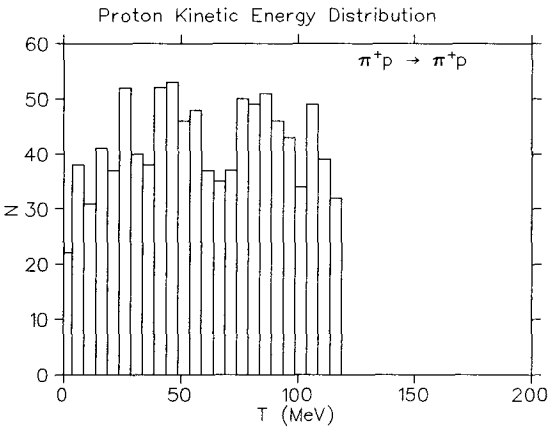

Figure 3.6

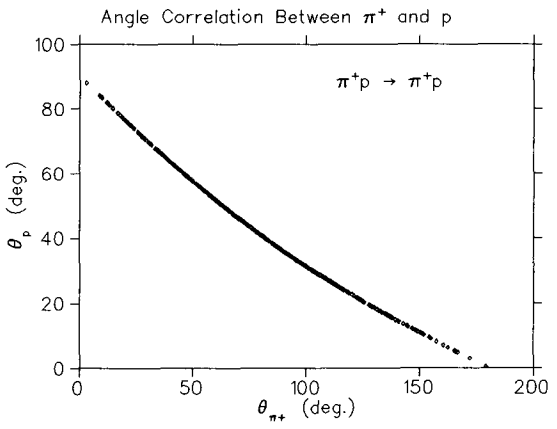

Figure 3.7

For reaction (2.3) $\pi^+p \rightarrow \pi^+\gamma p$, Figures 3.8-3.9 show a substantial overlap in the energy ranges of the outgoing π^+'s and protons with those of the principal reaction.

For reactions (2.4) $\pi^+p \rightarrow \pi^+\pi^+n$ and (2.5) $\pi^+n \rightarrow \pi^+\pi^-p$, the phase space distributions are almost identical to that of principal reaction, because the particle masses associated with these reactions are virtually identical to those of (2.1).

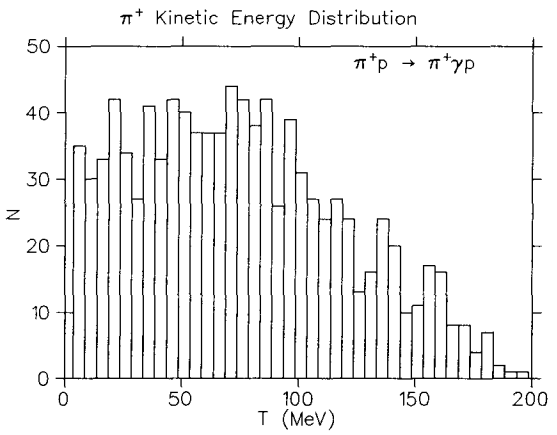

Figure 3.8

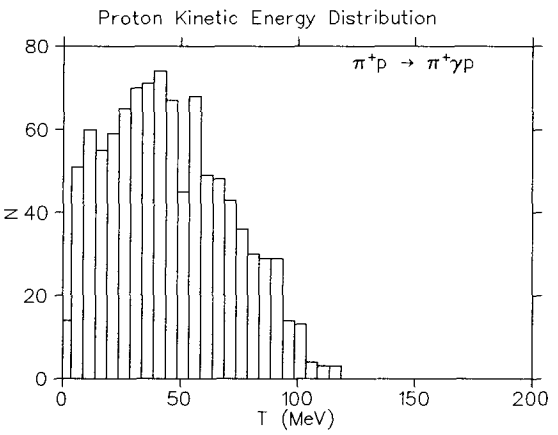

Figure 3.9

The conclusion that one comes to by considering the phase space distributions is the difficulty in measuring the reaction cross section of (2.1) since the energies of the outgoing particles are very simular. In the next section, a technique is proposed to measure the cross section of the principal reaction based on Monte Carlo simulation.

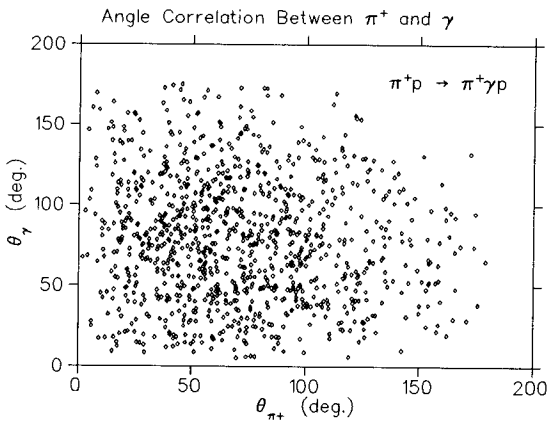

Figure 3.10

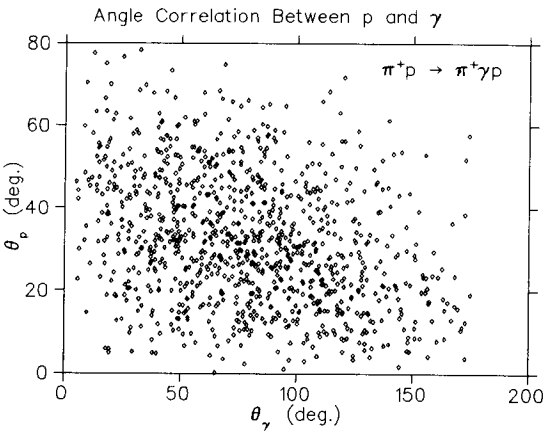

Figure 3.11

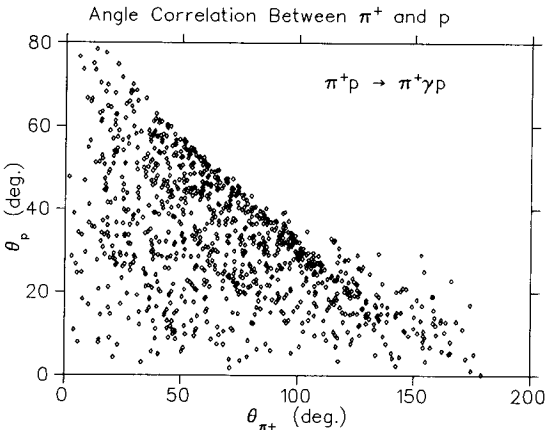

Figure 3.12

3.3 Simulation

Monte Carlo simulation of reactions (2.1)-(2.5) yield the following results in the ΔE vs E plane. For the analysis below, the acceptance angle for the S1-S2 array has been set to 30^0 (see sections 2.3, 2.4) and the incident pion kinetic energy, to 200.0 MeV. The total number events in the ΔE vs E plane are typically ~ 5000, based on 20 000 events 'Monte Carloed'. It will be shown below that the pile-up events can be used to measure the total cross section of reaction (2.1).

For reaction (2.1) $\pi^+ p \rightarrow \pi^+ \pi^0 p$, Figure 3.13 shows three distinct groups are present in the ΔE vs E plane. The lower band is created by π^+ particles while the higher band protons. The events outlined by the polygon window are the 'pile-up' events created by simultaneous π^+ and p hits of the S1-S2 detector (see section 2.4). The C veto (see section 2.2) has been disabled, for this figure. For Figure 3.15, the C veto has been activated; one can see that the middle proton band on Fig. 3.13 has disappeared in this plot as a result of a scattered π^+ triggering the C veto.

The question arises: where do the π^+'s in the lower pion band come from? The only π^+ that one should see are those that fall with the acceptance angle, and hence counted as a 'pile-up' event. The other π^+'s that fall outside the acceptance angle should simply not be counted. The π^+'s in the lower band *are* from 'pile-up' events. There are many pile-up events where the protons are of very low energies and gets stopped in S1 and hence one

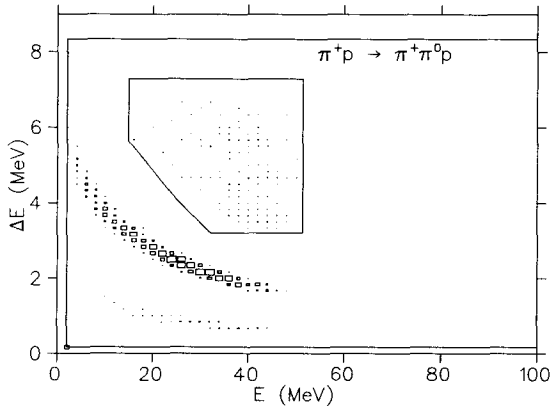

Figure 3.13 Reaction events in the ΔE vs E plane.

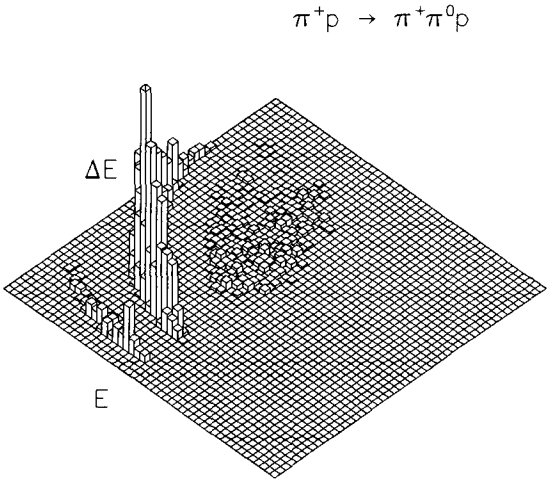

Figure 3.14 Surface plot of reaction events shown in Fig. 3.13.

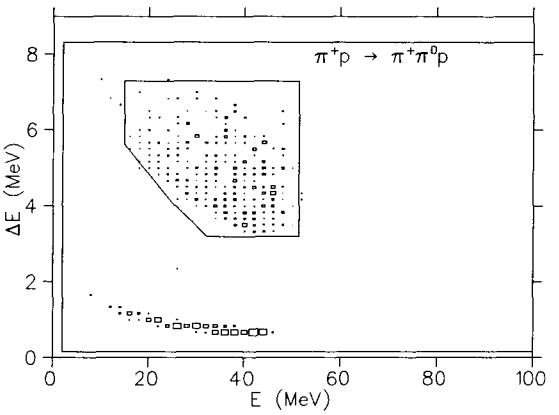

Figure 3.15 Reaction events in the ΔE vs E plane, with C veto enabled.

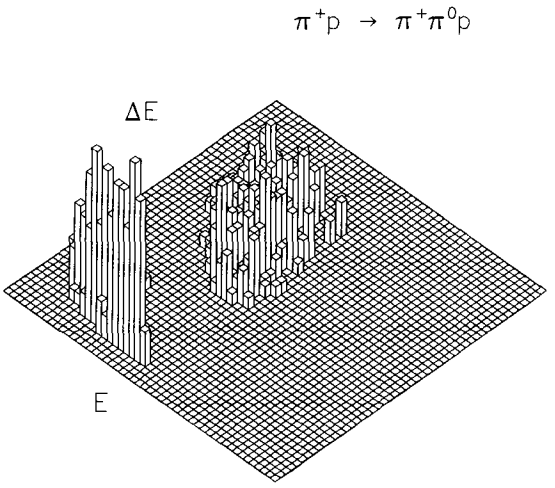

Figure 3.16 Surface plot of events shown in Fig. 3.15. (note: this Figure and Fig. 3.14 do not have common scales 'out of the ΔE vs E plane').

only sees the π^+ coming through both detectors. Such an event looks like a 'lone pion event'. There is no ambiguity associated with 'lone proton events' appearing in the proton band, since the phase space of the π^+'s is not restricted to the acceptance angle (see Fig. 3.4).

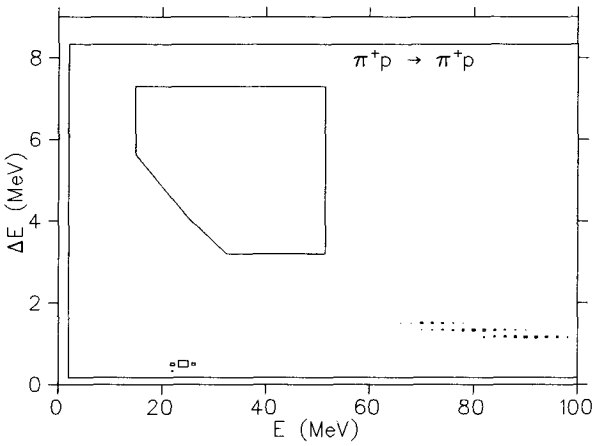

Figure 3.17 Elastic scattering background.

For the elastic channel (2.2) $\pi^+p \rightarrow \pi^+p$, Figure 3.17 shows that outgoing particles falling well away from, the 'pile-up window'. Hence, this background reaction is removed.

For (2.3) $\pi^+p \rightarrow \pi^+\gamma p$, Figures 3.18-3.19 show that events fall outside of the pile-up window.

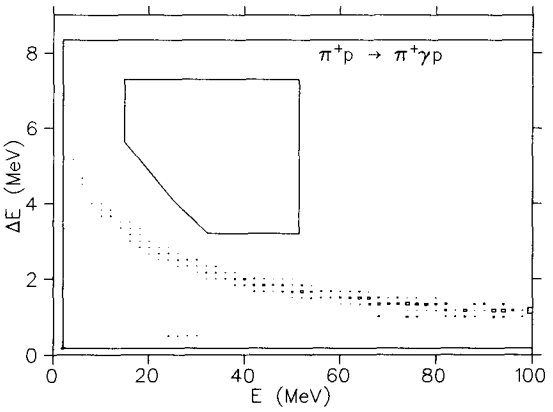

Figure 3.18

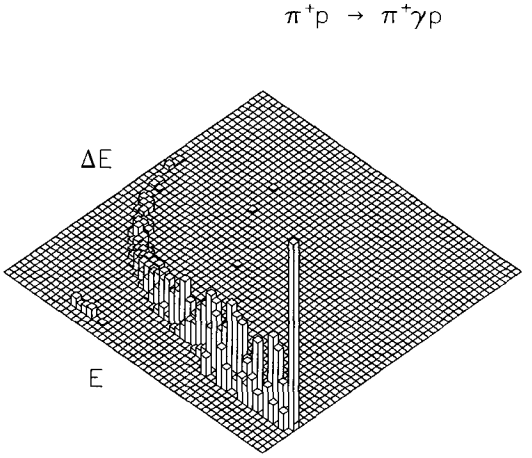

Figure 3.19

For the reaction (2.4) $\pi^+p \rightarrow \pi^+\pi^+n$, there is a pion band as well as a group of simultaneous $\pi^+\pi^+$; both features lie outside the pile-up window: (there is a single count in the pile-up window, which is considered negligible).

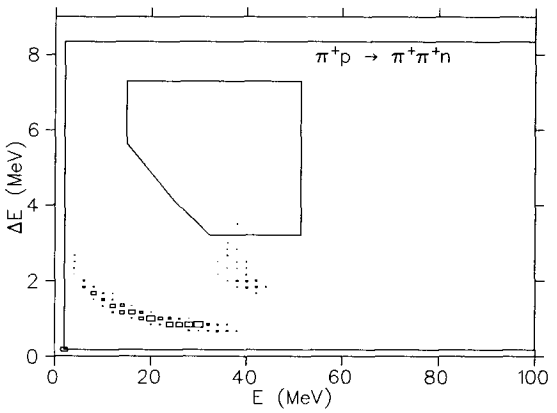

Figure 3.20

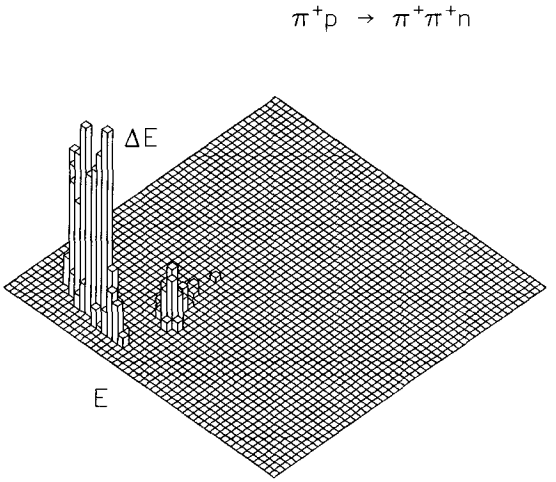

Figure 3.21

The background reaction (2.5) $\pi^+n \rightarrow \pi^+\pi^-p$, appears to cause the most difficulties. The phase space of this reaction is virtually identical to (2.1); as well, the reaction products on the right-hand side are almost the same. It is not suprising then that the signature of this reaction in the ΔE vs E plane (Fig. 3.22) looks very similar to that of the main reaction (Fig. 3.13). In particular, one sees that there is a significant number of events in the pile-up window, representing $\sim 27\%$ of the total cross section for this reaction. There is one important difference between this reaction and (2.1): both pions on the right-hand side are

charged. We will take advantage of this fact to eliminate this background. By using the cylindrical veto C most of the events from this reaction can be eliminated (Fig. 2.7). The no. of events now appearing in the pile-up window is approximately 0.7% of the total cross section. In principle, this method of removing the events from reaction (2.5) is redundant since the subtraction of CH_2 and C spectra (see sec. 2.3) should eliminate this background altogether. Nonetheless, we have chosen a more conservative route by eliminating events from this reaction *before* the subtraction. It is evident that the '0.7% of the total cross section' background mentioned above should be eliminated in the CH_2-C subtraction.

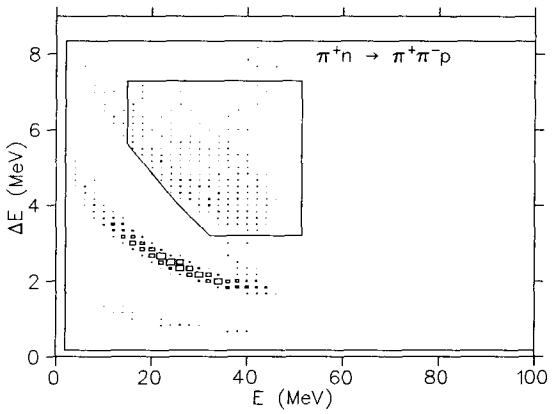

Figure 3.22

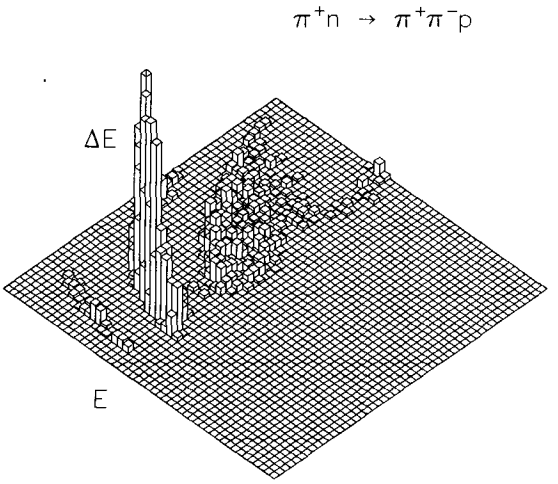

Figure 3.23

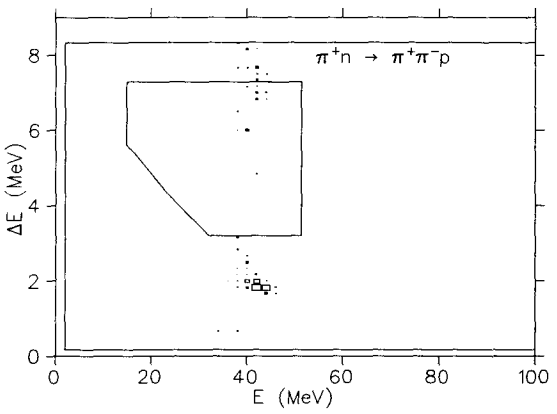

Figure 3.24

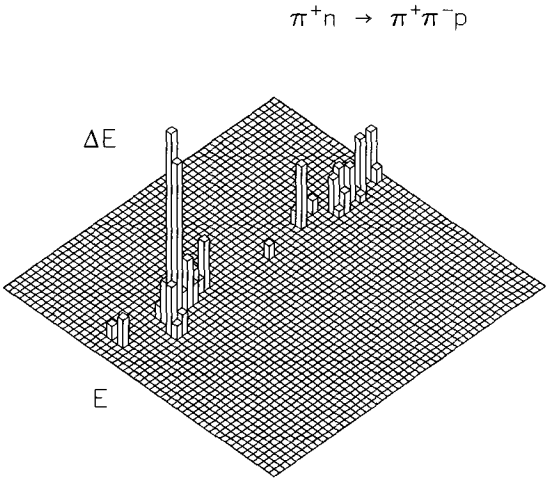

Figure 3.25

3.4 Conclusion

It is evident from the phase space of the different π^+p channels that it is very difficult to isolate the events from the principal reaction (2.1). We conclude that to measure the total cross section, one possible strategy is to consider the 'pile-up events' in the ΔE vs E plane. This strategy successfully isolates a fraction of the events from the principal reaction.

Chapter 4

The Experiment

4.1 Introduction

A feasibility study of the apparatus based on chapter 2 was performed at TRIUMF, on the M11 beam line during July and August of 1992. This chapter is devoted to highlighting what occurred during the experiment.

4.2 Initial Set-up: Additions and Modifications to Original Set-up

Even during the intial set-up, it was apparent that a large background signal was present due to the beam interaction with the S detectors. Therefore, several steps were taken to try and reduce this background and isolate the events coming from the target.

Absorber Introduced

It was discovered early on during set-up that protons that have leaked through along with the beam pions appeared in the S1 vs S2 plane. In order to eliminate this background, a 6 mm CH_2 absorber was introduced placed in front of the beam window (see Fig. 2.2).

The S2 Problem

Attached to the S2 detector, are 2 photomultiplier: S2-Left and S2-Right. During a trial run, it became apparent the signals from the S2-Left and S2-Right photomultipliers did not

match up: when the signal (No. of counts versus channel number) from one side was superimposed on the other, one signal was skewed relative to the other. This problem, as it was discovered, was a result of a rate dependance of the photomultipliers caused by a high voltage setting ($\sim$1800 V). The voltage was lowered and to compensate for this, an amplifier was used to boost the S2 signals.

Upon inspection of the S2-Left and S2-Right signals matching was achieved. However, while the matching problem was solved another problem with the S2 photomultipliers was transparent to the experimenters was discovered only during analysis of the data (discussed in Chapter 5).

S1 Threshold

Another technique was used to further lower the background events. The threshold of acceptance (discrimination level) was raised electronically on the S1 detector, to reject unwanted high energy events appearing away from the events in the 'pile-up' window.

S2 Detector Moved Downstream

To achieve better time-of-flight, the S2 and S3 detectors were moved 11 cm downstream[1]. It was not possible to further increase the time-of-flight because of the S2 detector size.

[1] The convention is that the beam starts 'upstream' from the beam pipe and proceeds 'downstream' through the target and detectors.

4.3 Running of the Experiment

Calibration

It is necessary to calibrate the S1-S2 array detectors: that is, to assign actually energies to the channels[2] corresponding S1 and S2 signals. The calibration was performed by sending pions and protons known energies through the S1-S2 array. Beam pions of 196.4 MeV and 'leaked-through' beam protons of 29.3 MeV were used. Both energies are the kinetic energies just before the target.

Main Runs

After the initial set-up, the main runs for attempting to measure the cross section took place at 2 different energies[3] 195.2 MeV and 201.2 MeV. Each run is about 10 hours long, with a total number of beam events of 10^{10}. A rough estimate of the cross section ($\sim 10\ \mu$b) suggests that the number of events from the principal reaction ~ 150 events at 195.2 MeV. The number of events at the higher energy is expected to be higher (perhaps a factor of two) since the cross section increases with energy (see Fig. 1.1).

---

[2] Channels here refer to the channels of the analogue to digital converters (ADC) used to record the signals.

[3] i.e., the kinetic energy of the incident π^+ at the center of the target.

4.4 Conclusion

In spite of the difficulties encountered during the intial set-up of the experiment is was possible to collect data at 2 different energies. In the next chapter, we will describe the analysis of the data and also the results extracted from the data.

Chapter 5

Experimental Results

5.1 Introduction

In this chapter, the method for analyzing data will be outlined; as well, the results from the experiment will be presented.

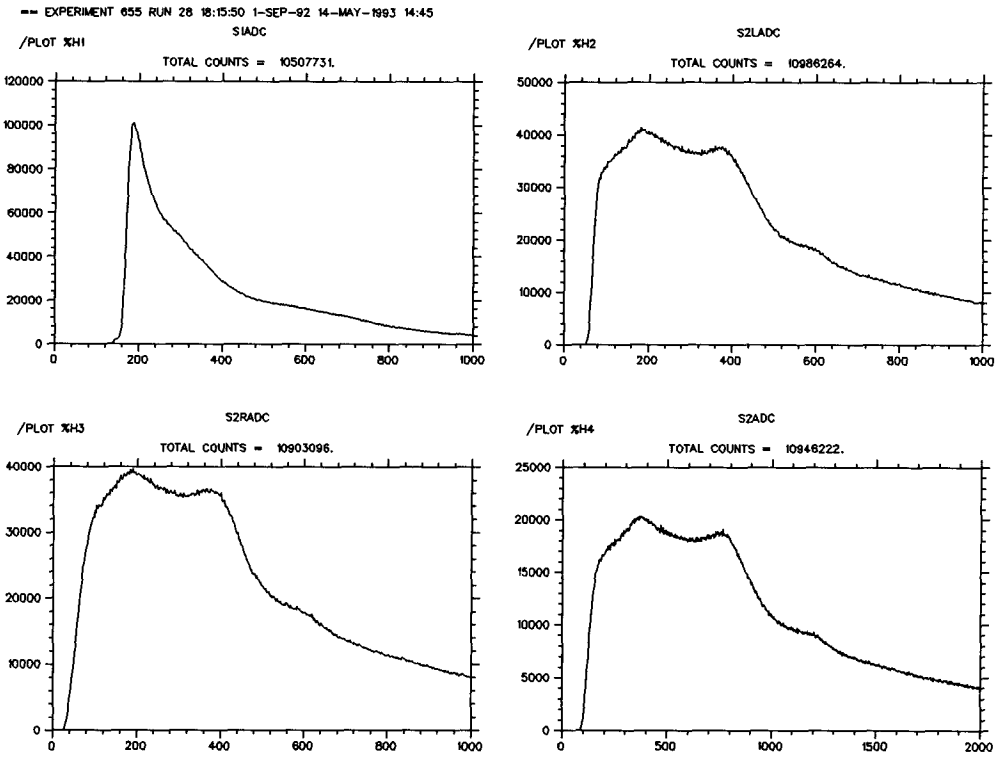

Figure 5.1 Typical spectra from a CH_2 target run. Vertical scales represent the number events; Horizontal scales represent energy in 'channel no.'.

5.2 Analysis of Data

The analysis of the results was performed using the TRIUMF software packages MOLLI, NOVA, FIOWA and REPLAY (see Appendix B).

The procedure is relatively simple: for a particular run, play back the data event by event and histogram the signals for the various detectors. Figure 5.1 shows the spectra from the S1 and S2 detectors for a typical run.

5.2.1 Time-of-Flight Cut

Figure 5.2 shows a detail of the time-of-flight spectrum between the B3 and S2. The spectrum identifies where events originate from along flight path across the experimental apparatus. The first two peaks describe events taking place in S2 and S1. The small bump of the right-hand side represents events coming from the target. However, it is clear that the 'tail' of the S1 and S2 peaks are superimposed on the target peak. The time-of-flight strategy is to introduced a limit of acceptance in time: e.g., only those events appearing with t > channel 350 are accepted. Such a 'cut' should eliminate most of the background events from S1 and S2. However, because the tails of S1 and S2 overlaps the target peak, there is no way, with the existing set-up to eliminate all the S1 and S2 events. In principal one can 'stretch' out the time-of-flight spectrum by increasing the distance between the target and each element (B3, S1, S2). But realistically one cannot get an arbitrarily large separation because of detector size limits and loss of event particles through the air. The limiting factor in the present feasibility study are the sizes of S1 and S2: to preserve the cone angle (see Fig. 2.1) for capturing all the protons from the principal reaction. The time-of-flight problem will be discussed in more detail in Chapter 6.

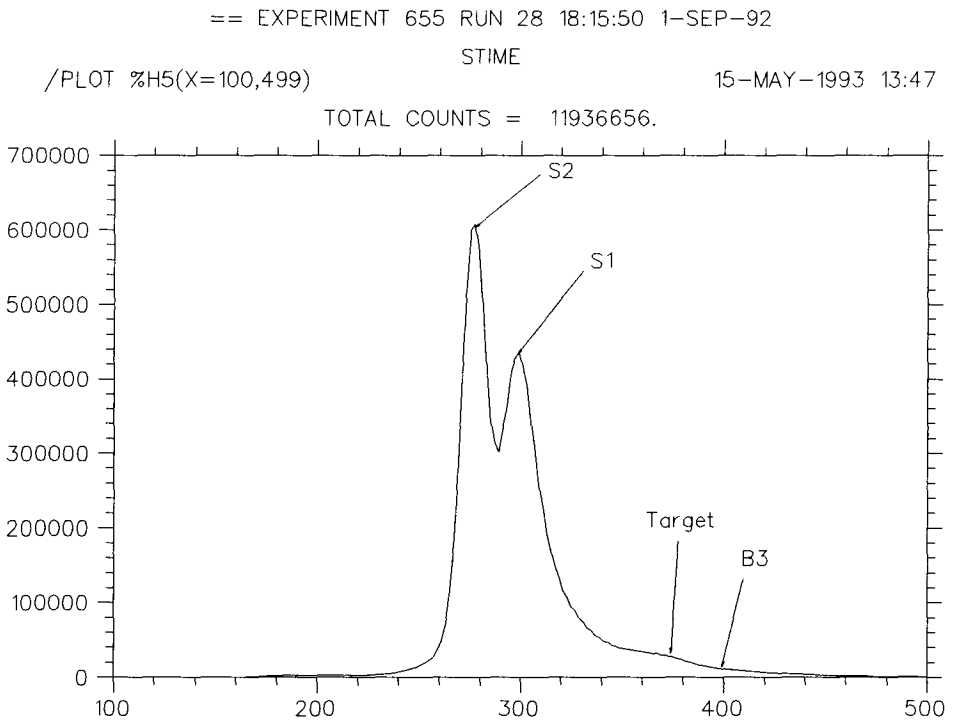

Figure 5.2 Detail of Time-of-Flight spectrum from a CH_2 target run. The vertical scale represents the no. of events while the horizontal represents time in 'channel no.' with each channel denoting 50 ps (picoseconds).

5.2.2 Events in the ΔE vs E Plane

Figure 5.3 shows the 2-diminensional spectra in the S1 vs S2 plane (ΔE vs E). Starting from the top left plot and progressing clockwise, the first plot is the 'raw' spectrum without a software time-of-flight cut. There is however, a hardware cut for all spectra introduced in S1 (see sec. 4.2) and hence no events appear below channel 120 of S1. The second and third plots are the spectrum with a time-of-flight cuts at channel 350 (see Fig. 5.2) and with the same cut but the S2-left signal only, respectively. For comparison the last plot shows

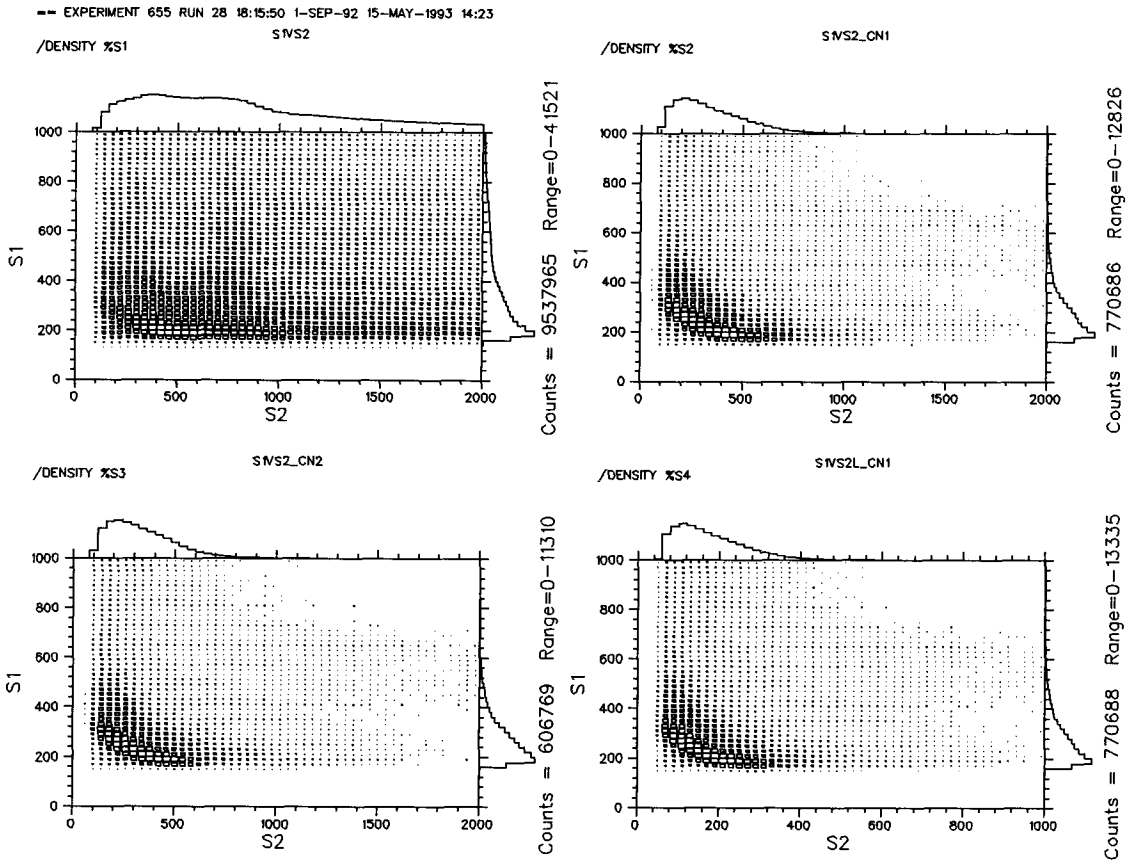

Figure 5.3 Typical S1 vs S2 spectra.

a spectrum with the time-of-flight cut at channel 375.

Figures 5.4-5.6 show first and second spectrum in more detail. Figure 5.4 (time-of-flight cut at channel 350) will be the one used in the attempt in extracting events from the principal reaction. This time-of-flight cut represents the maximum possible channel for rejecting S1 and S2 events but without undesirably rejecting target events. B3 events cannot be eliminated since its signature in the time-of-flight spectrum is much too weak.

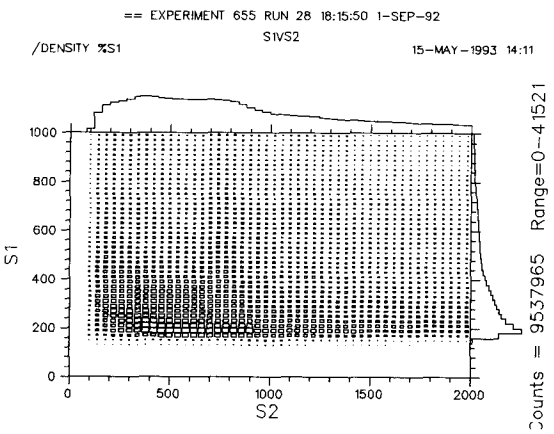

Figure 5.4 S1 vs S2 detail, raw spectrum.

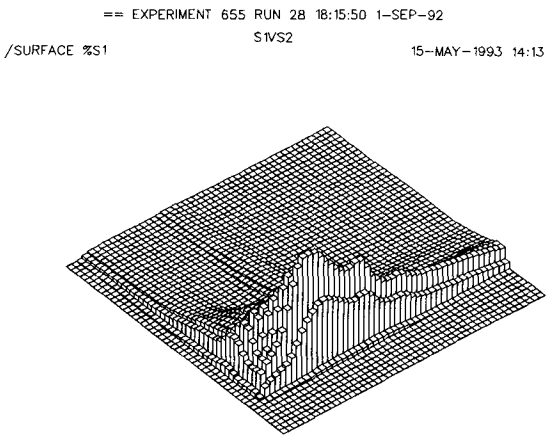

Figure 5.5 Surface plot of S1 vs S2, raw spectrum.

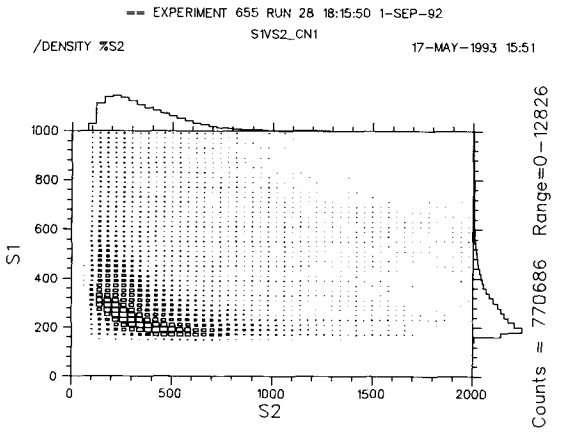

Figure 5.6 S1 vs S2 plot, with time-of-flight cut.

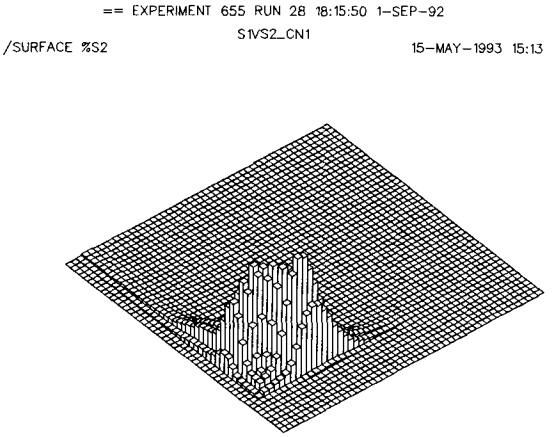

Figure 5.7 Surface plot of S1 vs S2 spectrum with time-of-flight cut.

5.2.3 Normalization of Spectra

In order to subtract C target spectra from those of the CH_2 target. One must account for the number of beam events[1] arising from 2 separate runs for the 2 different targets as well as the different number density of each target (i.e., the different number of scatterers).

Let I = no. of beam events[2]

N = number density of target particles in cm^{-3}

Δx = thickness of target in cm

n = $N\Delta x$, area density of target particles cm^{-2}

ΔI = no. of reaction events (or no. of particles scattered out of beam)

And, let the subscripts C, CH_2, H_2 denote the corresponding particles.

Then, the **normalized** spectra (per unit beam per unit scatterer) for H_2 is

$$\frac{\Delta I_{H_2}}{I_{H_2} n_{H_2}} = \frac{\Delta I_{CH_2}}{I_{CH_2} n_{CH_2}} - \frac{\Delta I_C}{I_C n_C} \tag{5.1}$$

[1] A beam event is defined as B1 AND B2 AND B3 AND (NOT V).

[2] There is an implicit time interval associated with I in the 'event by event' scenario.

But,

$$I_{H_2}=I_{CH_2} \qquad and \qquad n_{H_2}=n_{CH_2}$$

Because the H_2 molecules are bound to the C atom for the CH_2 molecule.

For data analysis, we rewrite (5.1) in the following form

$$\Delta I_{H_2}=\Delta I_{CH_2}-\frac{I_{CH_2}n_{CH_2}}{I_C n_C}\Delta I_C \tag{5.2}$$

Equation (5.2) gives the no. of H_2 events normalize with respect to a CH_2 run.

n can be calculated from

$$n=(N\Delta x)=\omega N_A \delta \tag{5.3}$$

where δ = $\rho\Delta x$, the thickness of the target in g/cm^2

N_A = Avagadro's number

ω = molecular weight in g

ρ = the density of the target in g/cm^3

For CH_2 : with δ_{CH_2} = 0.1480 g/cm^2 n_{CH_2} = 6.352 x 10^{21}cm^2

For C: with δ_C = 0.1824 g/cm^2 n_C = 9.166 x 10^{21}cm^2

5.3 Cross section

The total cross section σ (in cm^2) is given by the well known equation

$$\frac{\Delta I}{I} = \sigma N \Delta x = \sigma n \tag{5.4}$$

Where I = is the beam intensity in particles per unit time

ΔI = change in intensity

Δx = thickness of target in cm

N = number density target particles in cm^{-3}

n = area density of target particles in cm^{-2}

Hence, the total cross section for H_2 is essentially (5.1). The parameter η is introduced to account for the fact that only a fraction of the total cross section in measured because we are only considering events in the pile-up window.

$$\eta \sigma_{H_2} = \frac{\Delta I_{H_2}}{n_{H_2} I_{H_2}} \tag{5.5}$$

For a single proton, the cross section is

$$\sigma_H = \frac{\sigma_{H_2}}{2} \tag{5.6}$$

5.4 The CH_2-C Subtraction Spectra

The C target produces a simular set of spectra. As discussed in section 2.2, to obtain the H_2 cross section one must subtract the CH_2 spectra from C spectra. Figures 5.8 and 5.9 show the result of such a subtraction, with spectra normalized with respect to the CH_2 target run, eqn. (5.2). Figure 5.8 is a 'raw' subtraction without any time-of-flight cut introduced

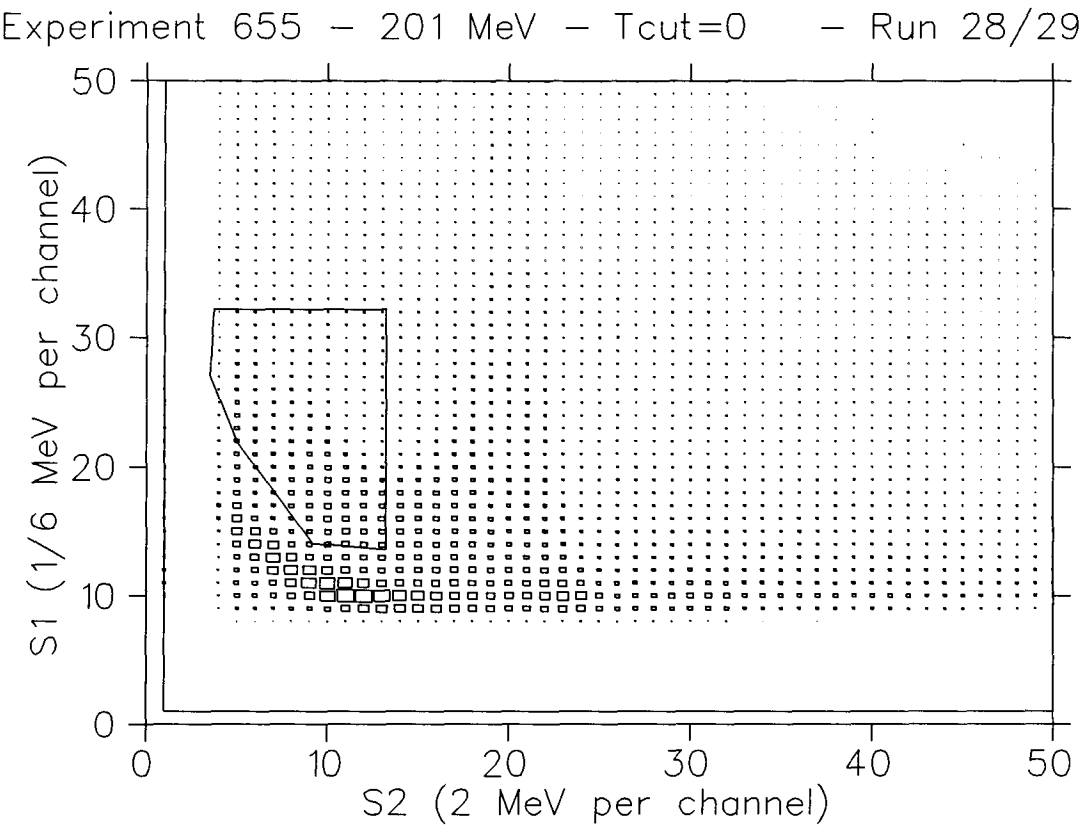

Figure 5.8 H_2 spectrum in the S1 vs S2 plane, with no time-of-flight cut. The total no. of events in the plane is 2 879 241, while in the pile-up window the no. of events is 364 556.

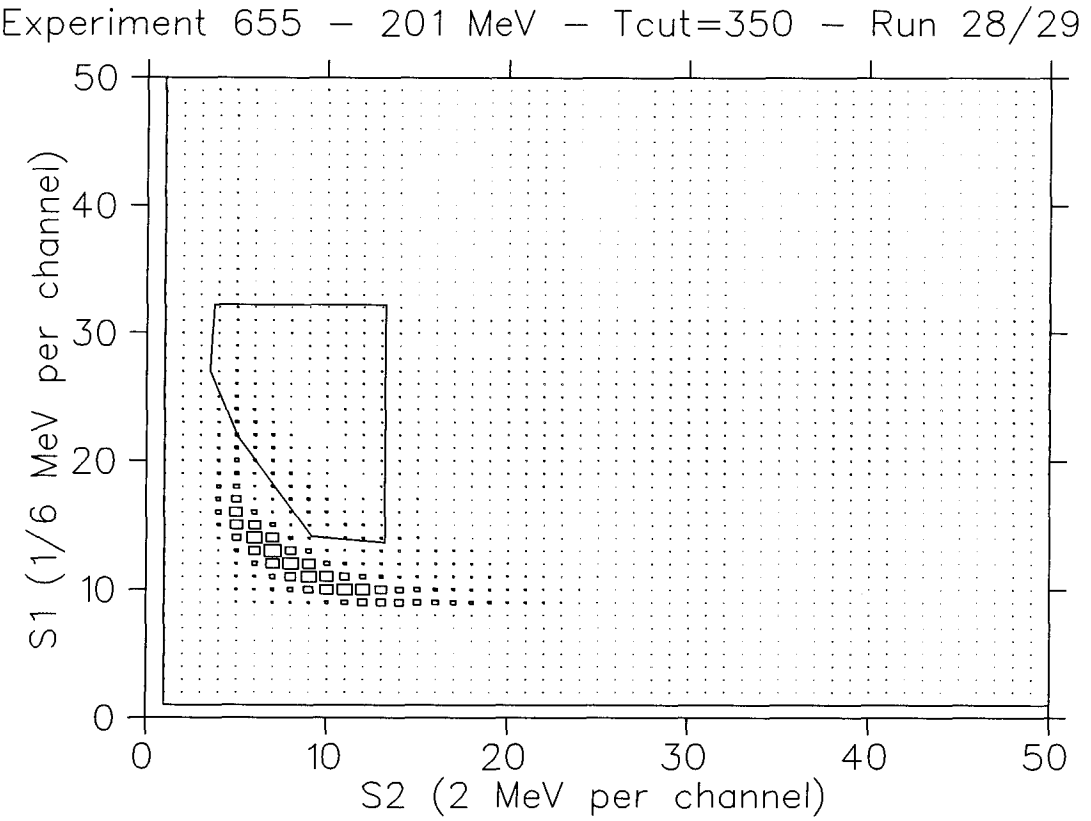

Figure 5.9 H_2 spectrum in the S1 vs S2 plane, with optimal time-of-flight cut. The total no. of events in the plane is 241 790 while in the pile-up window it is 32 019.

while Figure 5.9 represents the maximum possible cut. The time-of-flight cut has decrease the total number of counts in the entire plane by a factor of 12. While in the pile-up window, the events have decreased by a factor of 11. Nevertheless, the number of counts in the pile-up window is 32 019, which remains much higher than the expected number of events from the principal reaction.

Based on the number of beam events I_{CH_2} = 8.082673 x 10^9 for the CH_2 run, a total cross section of σ_H=10μb and η=0.15, a rough calculation using eqn. (5.5) shows that the number of events expected in the pile-up window is $\sim$150 events. Hence, the present background is some $\sim$200 times larger than the signal.

The large background is the result of events originating from the different detectors, especially S2 detector which is very thick (11cm). The strategy for removing the 'detector' events had only limited success since there was a lack of time-of-flight resolution for separating out the target events, due to the limitations of the present apparatus.

5.5 The Subtraction Problem

A serious problem was discovered during the analysis of the data. Subtraction of the CH_2 and C spectra yielded negative numbers in the S1 vs S2 plane. Figure 5.10 shows the negative contours in the S1 vs S2 plane for Fig. 5.9. The negative peak is at $\sim$100 counts. This peak does not appear to originate merely from random statistical fluctuations (i.e. noise) but rather from variation in the structure of the S signals. That is, the source of this problem originates from an instability of the S1 and S2 signals during successive runs. To illustrate this instability, let us consider the S1 and S2 signals from 4 different runs of the same Carbon target at the same energy (201 MeV). If the S signals are stable, then subtraction of the normalized spectra with respect to the number of beam events should

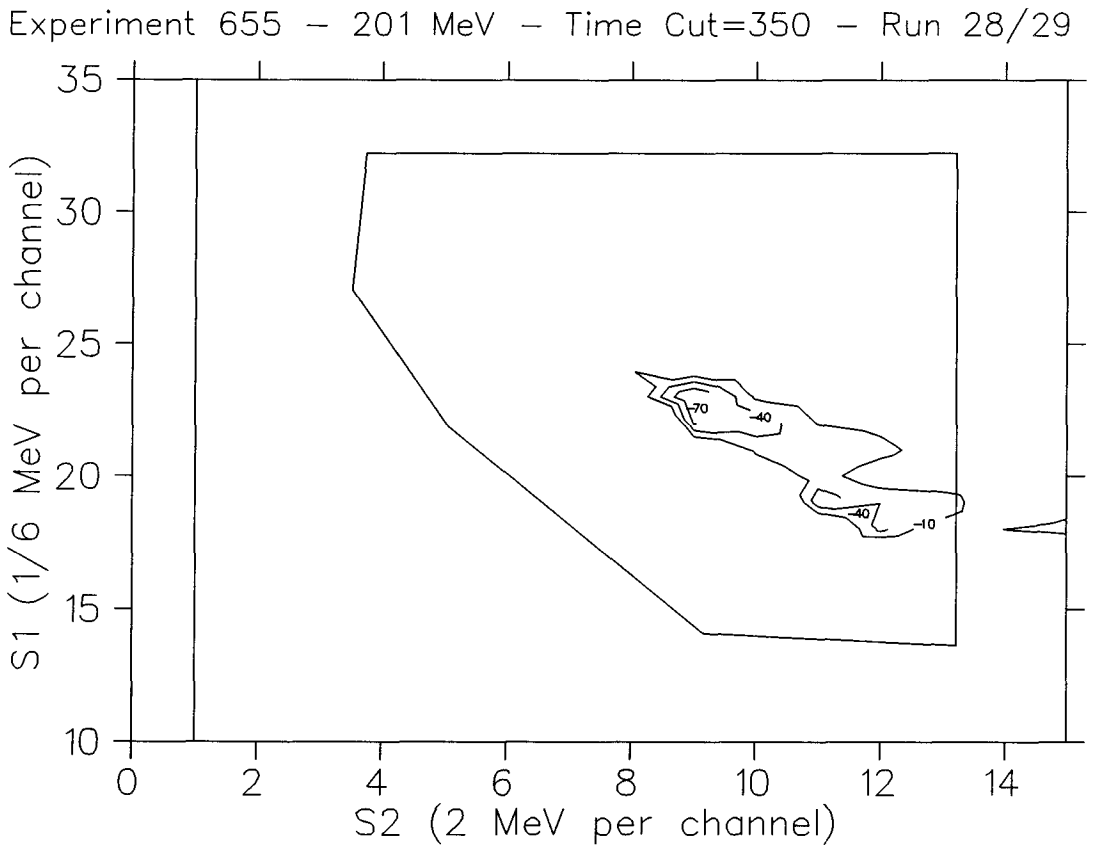

Figure 5.10 Negative contours in the S1 vs S2 plane.

yield a 'zero' result with some accompanying noise. Figures 5.11-5.14 show that no such matching exists. Two reasons have been proposed to account for the 'drift' in the S signals. First, the problem may orignate from instability in the photomultipliers. Second, the energy of the beam is drifting; it is known that the uncertainty in kinetic energy of the beam pions is ± 0.2 MeV, on the M11 beam line at TRIUMF. This subtraction problem remains unsolved and if the existing apparatus is used should be the subject of further study.

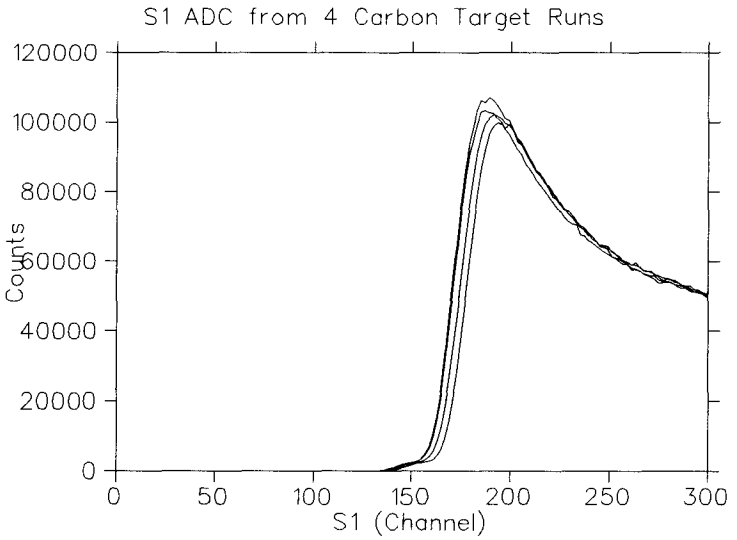

Figure 5.11 S1 Signal Instability.

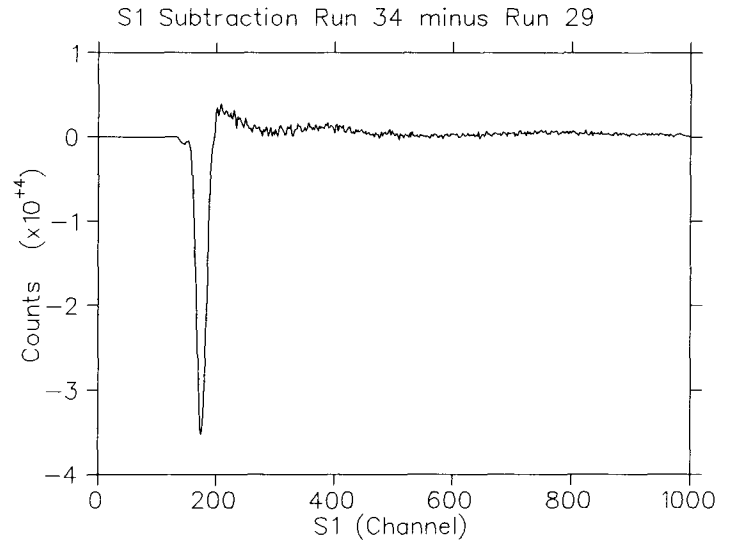

Figure 5.12 Subtraction of two S1 spectra, Run 34 minus Run 29.

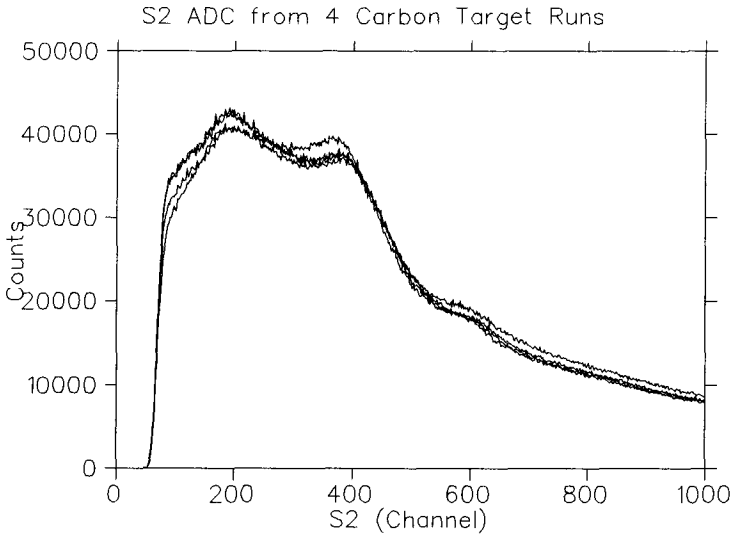

Figure 5.13 Instability in S2 signal.

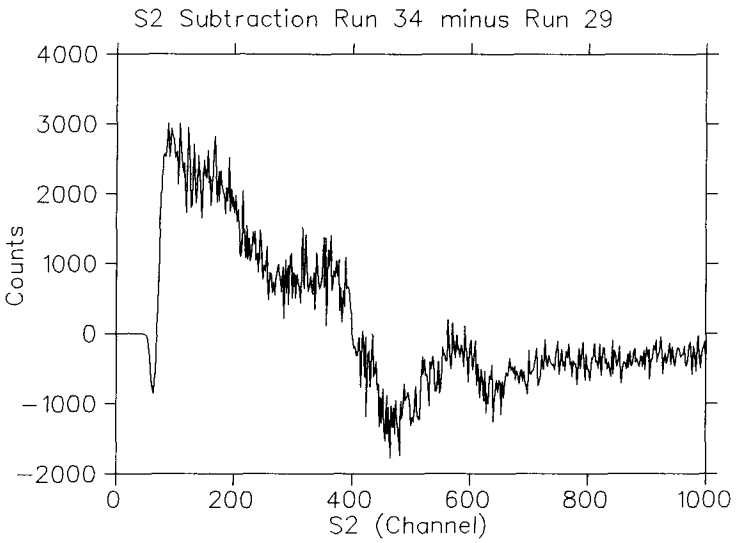

Figure 5.14 Subtraction of two S2 spectra, Run 34 minus Run 29.

5.6 Conclusion

From the present feasibility study, it is apparent that several problems need to be overcome: first the background will have to be decreased by 2-3 orders of magnitude and second, the stability of the S1-S2 detectors will have to addressed, before meaningful cross section measurements can be obtained. In the next chapter, different methods will be explored to improve on the present apparatus.

Chapter 6

Redesign of Experiment

6.1 Introduction

In this chapter, alternative ways of measuring the cross section of the principal reaction will be considered. Modifications to the original apparatus will be introduced.

6.2 Hole in the S1-S2 Telescope

As seen in the previous chapter the large number of reactions taking place in the S1-S2 detector has introduced a large background. One way to deal with this problem is to introduce a 'hole' in the center of both S1 and S2 and hence allow the beam to pass through the array without the possibility of interaction. There is however, a disadvantage to this technique: some of the legitimate 'pile-up' events will be lost. From phase space calculations, at an incident pion kinetic energy of 200 MeV, about 6.5% of pile-up events will be lost as a result of a hole equivalent to a 5^0 cone angle. Therefore, the parameter η (representing the percentage of total cross section measured) will be further reduced by 1 percent to 14%. Figure 6.1 shows the events lost for a 5^0 hole. The total number of events in the entire plane is 5000. The total number of pile-up events is 1106 and the total number of events lost as a result of the hole is 72.

Using Monte Carlo transport simulation, assuming the distance between the target and 'S' detectors is $\sim$1m, and a hole size of 5^0, about 2% of the beam interact with the 'S' detectors. Hence, we can estimate that the number of events in the pile-up window will decrease from 32 000 to 700 (using the sample run in sec. 5.1.5).

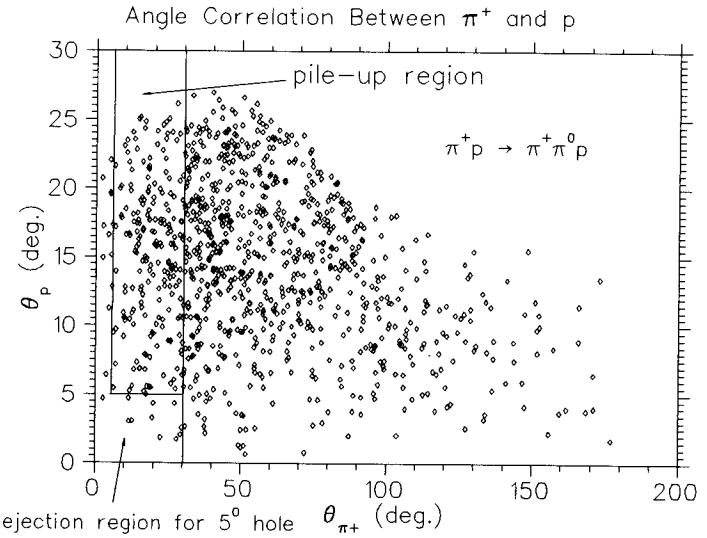

Figure 6.1 Angle correlation between outgoing pion and proton. The 'L' window in the lower left region represents events lost for a 5^0 hole.

There are two ways to introduce a 'hole' in the S detectors. One is to physically cut a hole. The difficulty in this technique is to assure that there will be proper light collection in the S detectors. The other is to introduce beam veto detectors much like B1, B2 and B3 downstream of the target and before the S1-S2 array. While the advantage to this technique is that one does not need to modify the S detectors, the disadvantage is that the veto detectors introduced will themselves have a background signature.

6.3 Increasing Time-of-Flight Separation

It is obvious that the larger the time-of-flight separation, the better events coming from the target will isolated from those of the detectors, particularly S1 and S2. However, the distance between the target and the S detectors cannot be arbitrarily large, since a 'dimininshing returns' phenomenon starts to take effect because the outgoing protons from the principal reaction get absorbed by air. For instance, at an incident pion kinetic energy of $T_{\pi+}=200$ MeV, the mean kinetic energy of the protons is ~ 30 MeV. At a distance of 0.775 m, half the protons will be lost. A way to reduce the effect of this problem may be to use a 'bag' of helium to fill the distance between the target and S1-S2. To get an idea how much the distance between the target and the S detectors needs to be increased, let us suppose that the incident π^+ kinetic energy is $T_{\pi+}=201$ MeV. To separate the 'peak' arising the target events (see Fig. 5.2), we need to shift the peak to the right by about 100 channels (5 ns). For complete isolation of the target 'peak', we use the fastest possible particle coming from the target which is a π^+ with kinetic energy of 201 MeV (elastic scattering) to determine the increase in distance needed to achieve this time-of-flight separation. The increase in distance needed is 1.37 m. Repeating the calculation with π^+'s with a kinetic energy of 60 MeV (these are the maximum kinetic energy π^+'s from the principal reaction), the increase in distance needed is 1.07 m. Clearly, it is not possible to let the outgoing particles from the reaction to travel through air since as shown above over half the pile-up events would be lost.

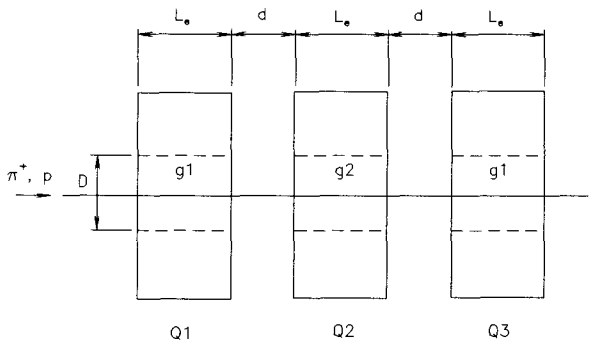

Figure 6.2 The triplet set-up.

6.4 Triplet Lens

With increased time-of-flight separation, not only does one runs into the problem of particle loss through air but also the requirement of large S1-S2 detectors. At a distance of 2 m, to cover a 30^0 cone angle the S detectors would have to be 1.07 m in diameter. One interesting method has been suggested to overcome both of these problems. Essentially, the method proposes to use a magnetic quadrapole triplet as a lense to focus outgoing event particles, keeping them within a reasonable size envelope downstream from the target. And by housing the triplet with a vacuum pipe, one can achieve a huge time-of-flight separation (a distance of $\sim$3 m between the target and S detectors can easily be achieved).

6.4.1 The Triplet Arrangement

Figure 6.2 shows the triplet set-up used for the simulation below. Each quadrapole (Q1, Q2, Q3) has a bore diameter of D=20.3 cm (8"), with a typical field gradient of g~0.6 KG/cm and effective length of L_e=0.49 m. The parameters that one adjusts are 'd' , the distance between the quadrapoles and 'g' the field gradient. For simplicity, a symmetric triplet will be used, i.e., the distance between Q1 and Q2 equals that between Q2 and Q3; and the field gradient in Q1 equals Q3.

6.4.2 The Triplet Simulation

To model the effect of the triplet on outgoing particles from the principal reaction, two software routines from TRIUMF was used: RAYTRACE[1] and REVMOC. The first routine makes use of a field map of the quadrapole triplet and raytraces particles through the system; the optics (focii, focal length, etc) of a particular triplet arrangement can be determined. Unfortunately, one needs to use a second routine to raytrace particles from the principal reaction because RAYTRACE can only handle very small particle divergences. REVMOC is a monte carlo beam transport program that performs the final raytrace with events from the principal reaction.

[1] Raytrace by Arthur Hayes, April 1980.

To summarize and elaborate on the method used:

1. Use RAYTRACE to find an optical set-up for a parallel stream of particles (e.g. protons) of fixed momentum. The optics of the system is then 'tuned' so that there is focusing in both transverse directions x and y. The focii for both transverse directions are made to coincide.
2. Duplicating the set-up from RAYTRACE, use REVMOC to raytrace events from the principal reaction.

Note: All analysis will performed in vacuum, at an incident pion kinetic energy of 200 MeV.

6.4.3 Results from the Simulation

Protons from the principal reaction are used to see the effect of the triplet. It is evident that the range of the momentum (10-340 MeV) and the range of the divergence ($\sim$ 0-30^0) are too large for a realistic size triplet lense to handle. For example, for quadrapoles with

bore diameter D=20.3 cm, 94% of protons gets rejected[2];

for bore diameter of D=30.5 cm, 88% gets rejected.

To see the effect of a smaller range of divergence, we limit the x and y divergences to be less than 5^0. For quadrapoles with

bore diameter D=20.3 cm, 63% of protons gets rejected;

for bore diameter of D=30.5 cm, 41% gets rejected.

[2] 'rejected' implies that a particle has drifted outside a cylinder defined by the quadrapole bore diameter.

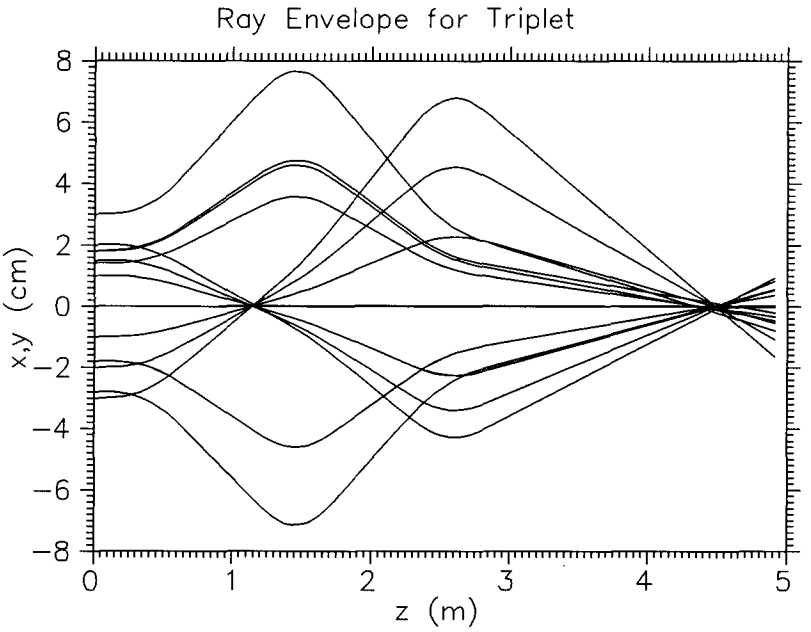

Figure 6.3 Raytrace of monoenergetic protons with T_p=36 MeV, zero divergence in the transverse (x,y) directions.

Plots from analysis with constraint of < 5^0 divergence

Triplet Tuning

Figure 6.3 shows the result of tuning the triplet set-up for a beam of monoenergetic protons with T_p=36 MeV. This energy was chosen because it is the mean energy of outgoing protons at an incident π^+ energy of $T_{\pi+}$=200 MeV. For convenience and without loss of generality, the proton beam is chosen to have zero divergence in the transverse (x,y) directions.

Note: 1. The triplet occupies the space z=(0.00, 2.92)m for this part of the analysis. Subsequent analysis will shift the triplet to another location in z.

2. The beam envelope with the single focus (divergent-convergent-divergent plane) is chosen to be the y direction.
3. The beam envelope with the double focus (convergent-divergent-convergent plane) is chosen to be the x direction.
4. Rays from both envelope converge at a focus at $z \sim 4.43$ m.

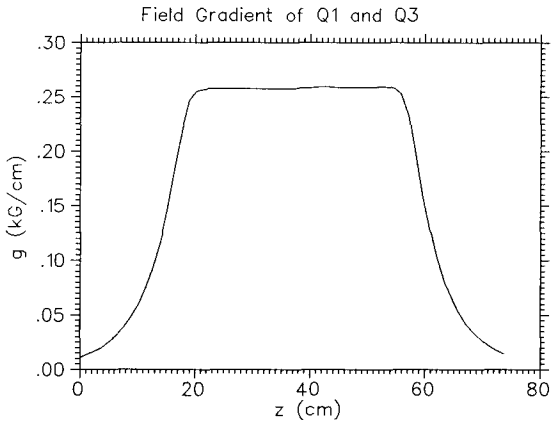

Figure 6.4 Field gradient of Q1 as a function of axial distance z. Q3 has an identical field gradient.

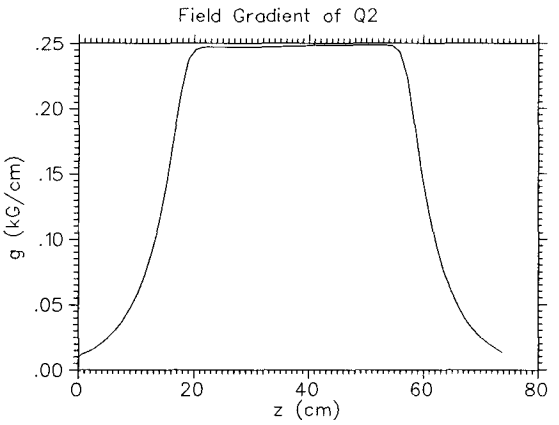

Figure 6.5 Field gradient of Q2, as a function of z.

The settings for focusing as shown in Figure 6.3 are

d=60.0 cm g1=0.258 kG/cm g2=0.248 kG/cm.

Figures 6.4 and 6.5 show the field gradient of each quadrapole with these settings.

Raytrace with protons from the principal reaction

Figures 6.6 and 6.7 show the result of the monte carlo simulation for a triplet with the above settings. The two vertical lines define the location of the triplet, z=(1.53,4.45) m, which is different from the previous location along z axis. It is apparent that even restricting the particles to divergences of less 5^0, the beam envelopes are still unrealistically large.

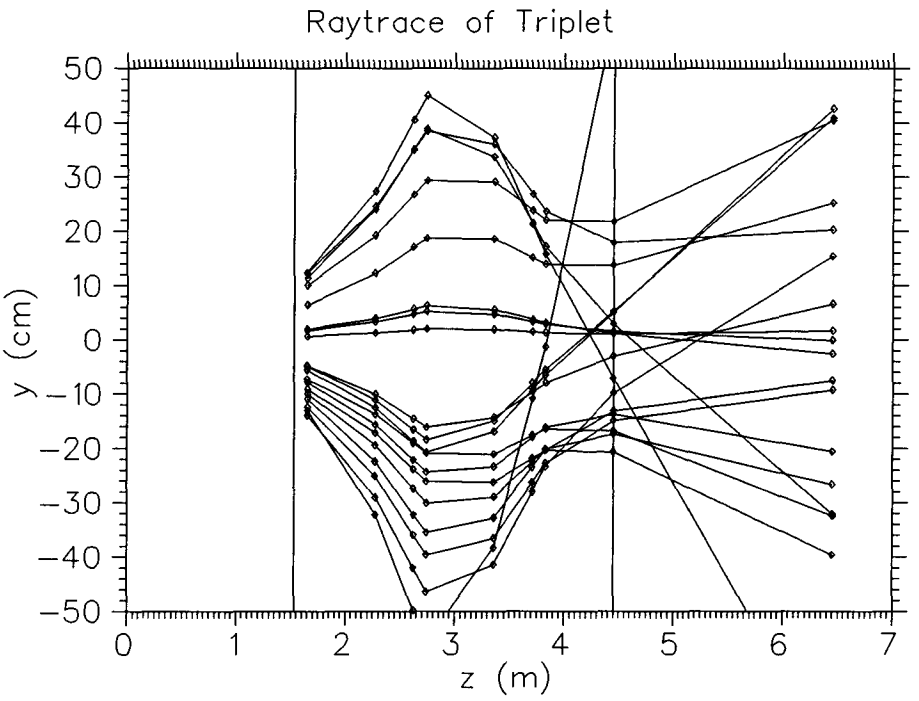

Figure 6.6 Raytrace of outgoing protons from the reaction $\pi^+p \rightarrow \pi^+\pi^0p$, with divergence in the x,y directions < 5^0 (dcd plane).

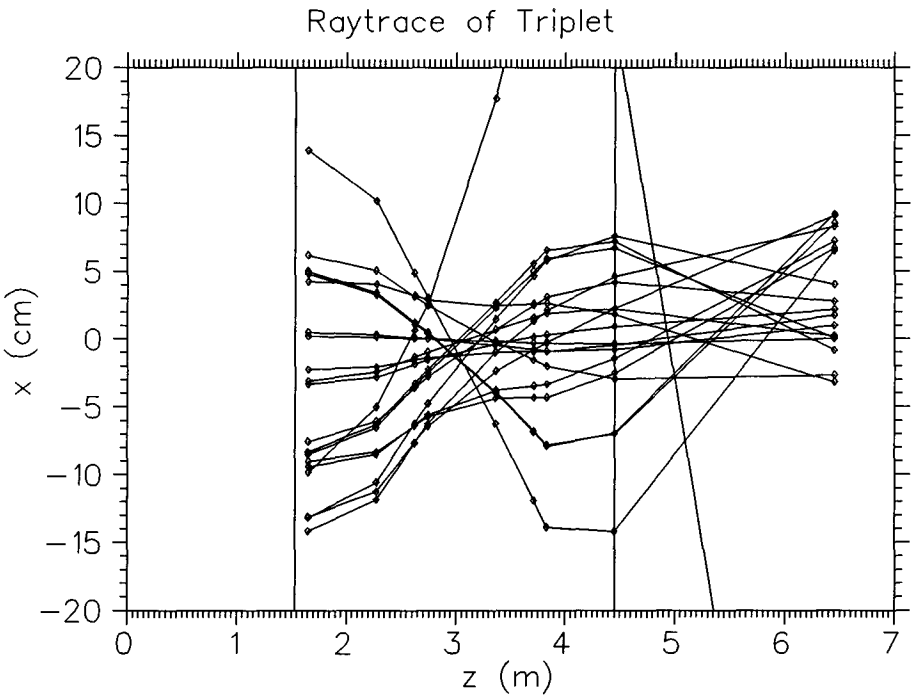

Figure 6.7 Raytrace of protons from the reaction $\pi^+ p \rightarrow \pi^+ \pi^0 p$, with divergence in the transverse directions < 5^0. This figure shows the x direction (cdc plane).

6.5 Conclusion

In this chapter, several methods have been proposed to improve on the current set-up. Introducing a hole in the S detectors and increasing the time-of-flight separation remain two feasible methods in dealing with the background. Preliminary calculations show very impressive reductions in the background by implementing these methods. Nonetheless, these calculations only suggest that the background appears to be within the same order as the events of interest. It is difficult, if not impossible to test out these methods without further experimentation. It was also shown in this chapter that the triplet lens will not be useful in helping the gain more time-of-flight separation since the outgoing particle envelope remain unrealistically large.

Chapter 7

Final Conclusions

A feasibility study for measuring the total cross section for the π-2π reaction, $\pi^+ p \rightarrow \pi^+ \pi^0 p$ was performed. The data collected was not useful in extracting the total cross section. However, the data was useful in accessing the background events for the existing apparatus. The background signal is 2-3 orders of magnitude larger than the 'reaction' signal. Several ways were introduced to help reduce the background: however, it was not possible to state conclusively that these methods will reduce the background sufficiently to extract a cross section measurement without further experimentation. In chapter one, we also showed the motivation for performing this experiment in the context of chiral perturbation theory which suggests that in order for this reaction to be useful in extracting information about π-π scattering, the experimental error for the total cross section must be less than $\sim \pm 10\%$. This constraint poses another challenge for measuring the total cross section for this reaction.

Bibliography

[1] Steven Weinberg, Phys. Rev. Lett. **17** (1966) 616.

[2] Martin Sevior et al., Phys. Rev Lett. **66** (1991) 2569.

[3] Neil Fazel, M.Sc. Thesis (1992) University of British Columbia, unpublished.

[4] Eli Friedman, Triumf Research Proposal, Experiment 655 (1991), unpublished.

[5] Eli Friedman et al., Phys. Lett. **231B** (1988) 39.

[6] Eli Friedman et al., Nucl. Phys. A in press.

[7] Eli Friedman, Triumf Research Proposal, Experiment 598 (1990), unpublished.

[8] Eli Friedman et al Phys. Lett. **302B** (1993) 18.

[9] J.D. Jackson, *Classical Electrodynamics*, 2nd ed., John Wiley, Chapter 13 (1975)

[10] Yu. A. Batusov et al., Sov. J. Nucl. Phys. **21** (1975) 162;
Sov. J. Nucl. Phys. **1**, (1965) 374.

[11] M. Arman et al., Phys. Rev. Lett. **29** (1972) 962.

[12] B.R. Martin, D. Morgan and G. Shaw, *Pion-Pion Interactions in Particle Physics*, Academic (1975).

[13] Steven Weinberg, Phys. Rev. Lett. **18** (1967) 188.

[14] J. Schwinger, Phys. Lett. **24B**, (1967) 473.

[15] M.G. Olsson and L. Turner, Phys. Rev. Lett. **20** (1968) 1127.

[16] M.G. Olsson and L. Turner, Phys. Rev. **181** (1969) 2141.

[17] J. Gasser and H. Leutwyler, Phys. Letters **125B** (1982) 312.

[18] A.N. Ivanov and N.I. Troitskaya, Sov. J. Nucl. Phys. **43** (1986) 260.

[19] J. Lowe et al., Phys. Rev. C **44** (1991) 956.

[20] M.G. Olsen et al., Phys. Rev. Lett. **38** (1977) 296.

[21] D. Mark Manley, Phys. Rev. D **30** (1984) 536.

[22] E. Oset and M. Vicente-Vacas, Nucl. Phys. A 446 (1985) 584.

[23] J. Gasser and H. Leutwyler, Phys. Rep. **87** (1982) 77.

[24] J. Gasser and H. Leutwyler, Phys. Lett. **125B** (1983) 325.

[25] J. Gasser and H. Leutwyler, Phys. Lett. **125B** (1983) 321.

[26] A.V. Kravtsov et al., Nucl. Phys. B **134** (1978) 2622.

[27] J. Gasser and H. Leutwyler, Ann. Phys. (N.Y.), **158** (1984) 142.

[28] J.F. Donoghue et al., Phys. Rev. D **38** (1988) 2195.

[29] V. Sossi, Phys. Lett. B **298** (1993) 287.

[30] V. Barnes et al., CERN Report 63-27 (1963).

Appendix A

Electronics

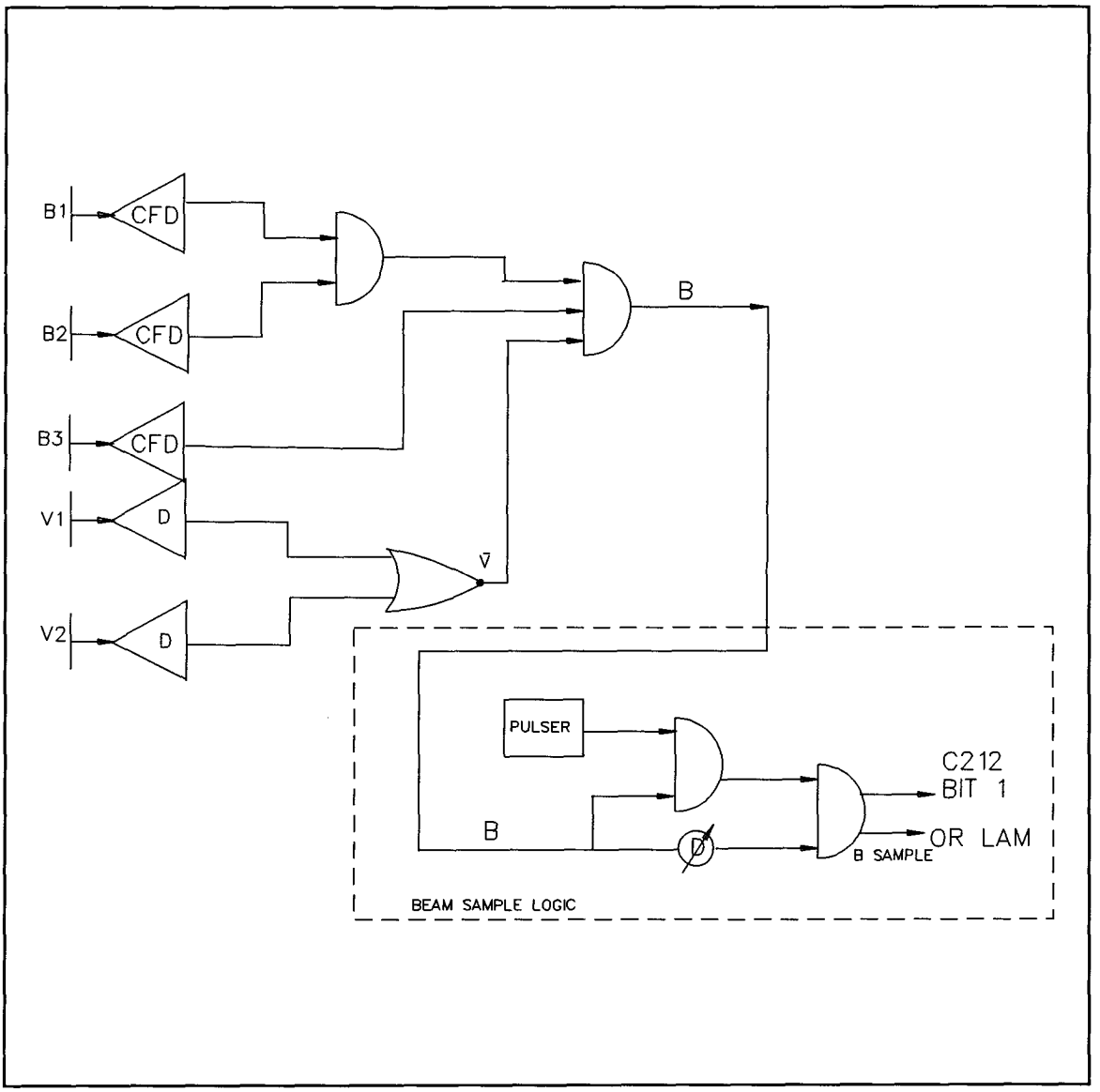

Figure A.1 Block diagram of 'beam' logic.

Appendix A. Electronics

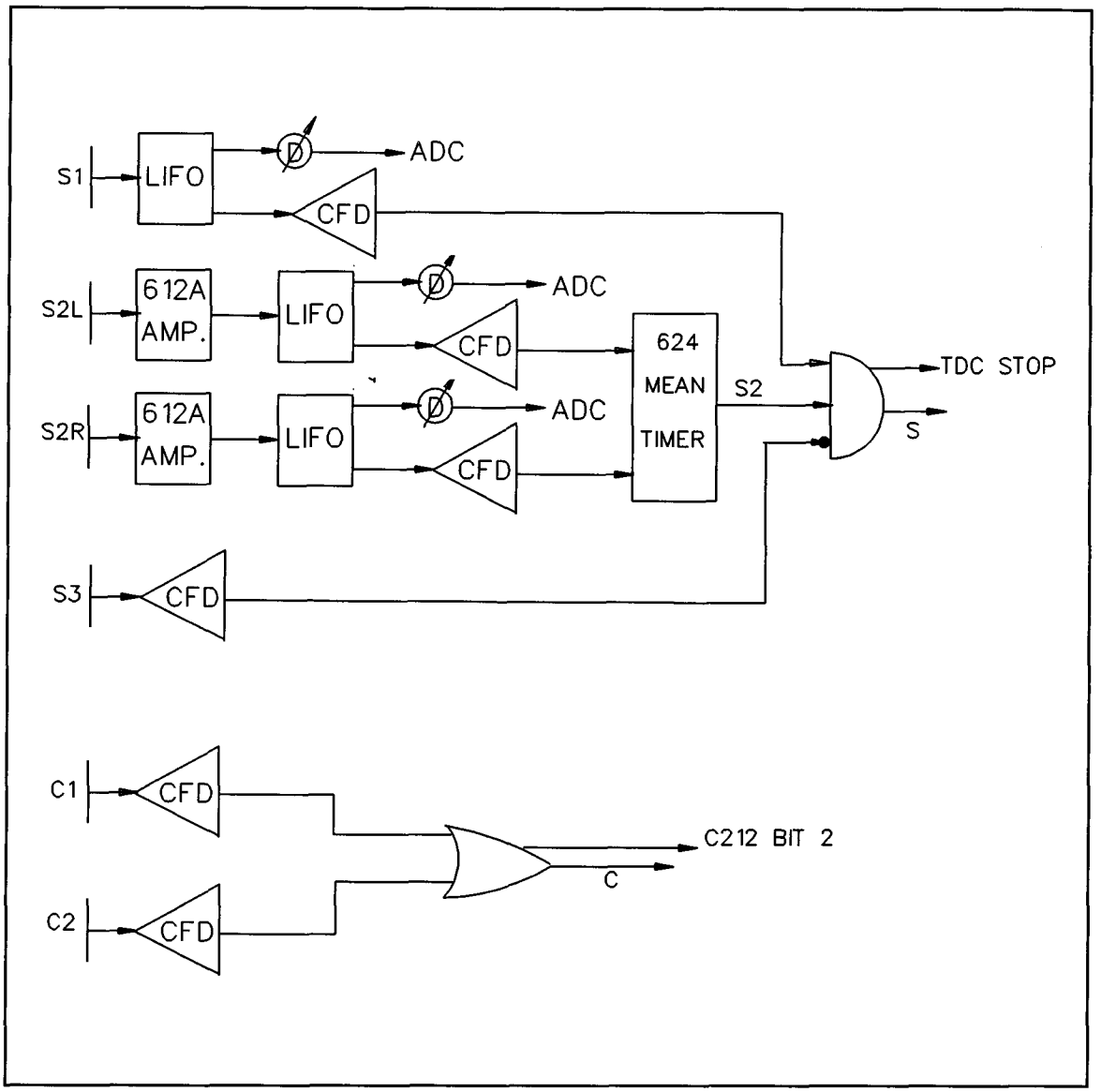

Figure A.2 Block diagram of 'detector' logic.

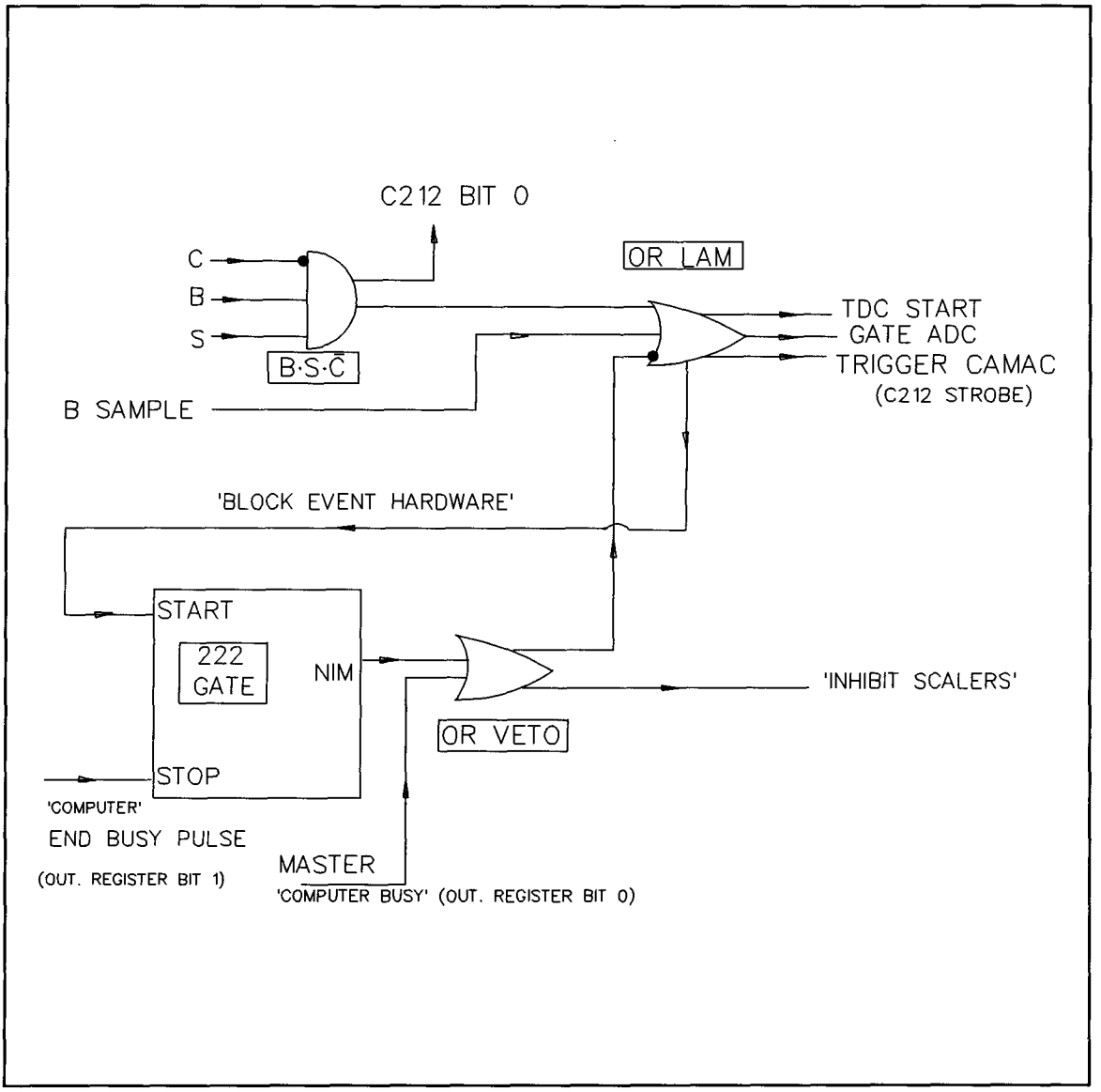

Figure A.3 Block diagram of 'event' logic.

Appendix A. Electronics

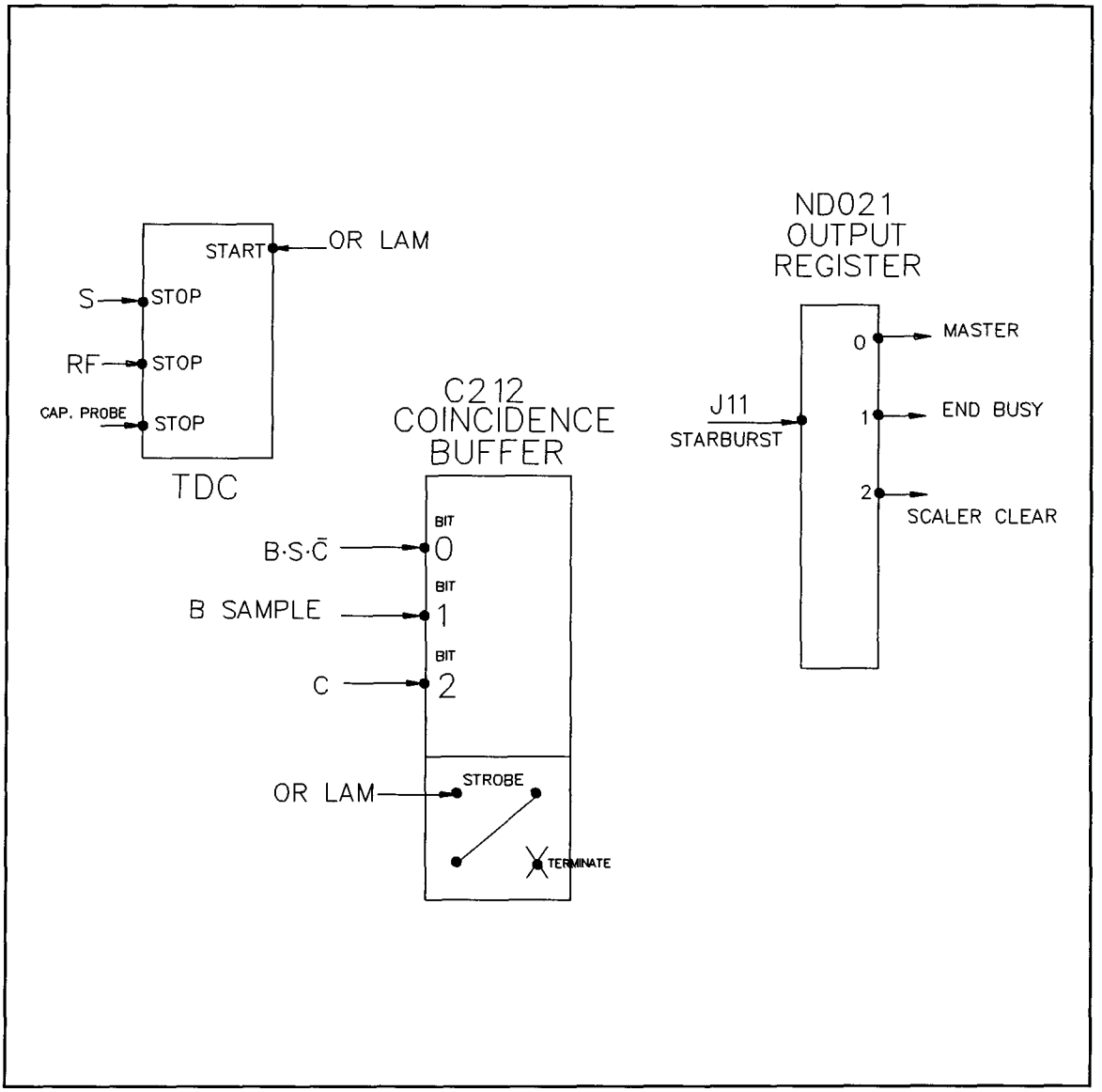

Figure A.4 Various modules.

Appendix B

Analysis Software

Listing of Routines for Driving MOLLI[1]

There are 3 routines (define, dplot and scalers) in 3 source files (define1.for, dp2.for, and sca.for).

define1.for

```
C this version is for multiple time cuts analysis
C
      SUBROUTINE DEFINE
C
C
      CALL PTITLE1('EXPERIMENT 655')
      CALL PTITLE2('RUN NO. ')
C
C DETECTOR HISTOGRAMS
C
      CALL THIST(1,'S1ADC$')
      CALL PHIST(1, 0.0, 2.0, 500, 0)
C
      CALL THIST(2,'S2LADC$')
      CALL PHIST(2, 0.0, 2.0, 500, 0)
C
      CALL THIST(3,'S2RADC$')
      CALL PHIST(3, 0.0, 2.0, 500, 0)
C
      CALL THIST(4,'S2ADC$')
      CALL PHIST(4, 0.0, 2.0, 1000, 0)
C
C**********************************************************************
C S1 VERSUS S2 HISTOGRAMS
C
      CALL TSCAT(1,'S1VS2 @S2@S1@$')
      CALL PSCAT(1, 0.0, 40.0, 50 , 0.0, 20.0, 50)
C
```

[1] MOLLI stands for 'Multi Offline Interactive Analysis' and is a software package for offline analysis of data. for more information see the documentation titled 'MOLLI' by Anne W. Bennett (1983) and Corrie Kost (1985).

Appendix B. Listing of Routines for Driving MOLLI

```
C
      CALL TSCAT(3,'S1VS2_CN2 @S2@S1@$')
      CALL PSCAT(3, 0.0, 40.0, 50 , 0.0, 20.0, 50)
C
      CALL TSCAT(4,'S1VS2L_CN1 @S2@S1@$')
      CALL PSCAT(4, 0.0, 20.0, 50 , 0.0, 20.0, 50)
C
      CALL TSCAT(5,'S1VS2R_CN1 @S2@S1@$')
      CALL PSCAT(5, 0.0, 20.0, 50 , 0.0, 20.0, 50)
C
      CALL TSCAT(6,'S1VS2L_CN2 @S2@S1@$')
      CALL PSCAT(6, 0.0, 20.0, 50 , 0.0, 20.0, 50)
C
      CALL TSCAT(7,'S1VS2R_CN2 @S2@S1@$')
      CALL PSCAT(7, 0.0, 20.0, 50 , 0.0, 20.0, 50)

C**********************************************************************
C TIME OF FLIGHT HISTOGRAMS
C
      CALL THIST(5,'STIME$')
      CALL PHIST(5, 0.0, 2.0, 1000, 0)
      CALL THIST(6,'TCAP$')
      CALL PHIST(6, 0.0, 2.0, 1000, 0)
      CALL THIST(7,'TRF$')
      CALL PHIST(7, 0.0, 2.0, 1000, 0)
C
      RETURN
      END
```

Appendix B. Listing of Routines for Driving MOLLI

dp2.for

```
C this version is for multiple time cuts analysis
C  SUBROUTINE DPLOT
C
C
C-----------------------------------------------------------------------
C
      SUBROUTINE DPLOT
C
C
      COMMON /EVENT/ RAW(50)
C       COMMON /IREC/  IRAW(50)
C
      REAL*4 TCUT1 /350.0/
      REAL*4 TCUT2 /360.0/
C       REAL*4 TCUT3 /375.0/
      INTEGER*4 EMASK /1/
      INTEGER*4 BMASK /2/
C
      REAL*4 S1ADC, S2LADC, S2RADC, S2ADC
      REAL*4 STIME, CAP_PRB, RF
      INTEGER*4 BITS
      INTEGER*4 EVENT, BSAMPLE
C
      S1ADC=RAW(2)
      S2LADC=RAW(5)
      S2RADC=RAW(4)
      S2ADC=S2LADC + S2RADC
C
      STIME=RAW(7)
      CAP_PRB=RAW(8)
      RF=RAW(9)
C
      BITS=RAW(11)
      EVENT= (EMASK .AND. BITS)
      BSAMPLE= (BMASK .AND. BITS)
C       WRITE(6,*) BITS,EVENT,BSAMPLE
C
      IF (EVENT .EQ. EMASK) THEN

        CALL HIST(S1ADC, 1., 1)
        CALL HIST(S2LADC, 1., 2)
        CALL HIST(S2RADC, 1., 3)
        CALL HIST(S2ADC, 1., 4)
        CALL HIST(STIME, 1., 5)
C
        CALL SCAT(S2ADC, S1ADC, 1. , 1)
          CALL SCAT(S2LADC, S1ADC, 1. ,4)
```

```
        CALL SCAT(S2RADC, S1ADC, 1. ,5)

C
      IF (STIME .GT. TCUT1) THEN
        CALL SCAT(S2ADC, S1ADC, 1. , 2)
      END IF
C
      IF (STIME .GT. TCUT2) THEN
        CALL SCAT(S2ADC, S1ADC, 1. , 3)
        CALL SCAT(S2LADC, S1ADC, 1. ,6)
        CALL SCAT(S2RADC, S1ADC, 1. ,7)

      END IF
    END IF
C
    IF (BSAMPLE .EQ. BMASK) THEN
C
      CALL HIST(CAP_PRB, 1., 6)
      CALL HIST(RF, 1. , 7)
    END IF
    RETURN
    END
```

Appendix B. Listing of Routines for Driving MOLLI

sca.for

```
      SUBROUTINE SCALERS (*,*,*)
C=====================================================================
C==   Suen version
C==   To fill the scaler values
C=====================================================================
C
      IMPLICIT NONE

      include 'molli$DIR:scalers.inc'
      include 'molli$DIR:molli_units.inc'
      include 'molli$DIR:mflags1.inc'
      include 'molli$DIR:pointer.inc'
      include 'molli$DIR:irec.inc'

      INTEGER*2 INT2(2)
      INTEGER*2 MASK(6)/1,2,4,8,16,32/
      INTEGER*4 KOVER/16777216/
C
C default integer declaration in INTEGER*4
C
      INTEGER   INT4, NWORD, IPOINT, IVAL, K, I, J, NVALUE
      EQUIVALENCE (INT2(1),INT4)

C=====================================================================
C==   Each scaler uses 2 INTEGER*2 words in IREC.
C==   These are combined to a single INTEGER*4 word in SCALER
C==   Ignore this Type SCALER event if it is the first event of a run
C=====================================================================
      INT2(1)=IREC(KOUNT+4)
      INT2(2)=IREC(KOUNT+5)
      IF(INT4.EQ.1)RETURN

      NWORD=IREC(KOUNT+1)/2
      NBLOCK=(NWORD-5)/14

      IF(NBLOCK.LT.1)RETURN

      IF(NBLOCK.GT.n_scal_m)THEN
        WRITE(prunits(1),50)NBLOCK,n_scal_m
        If(log)WRITE(prunits(2),50)NBLOCK,n_scal_m
50      FORMAT('0Type "SCALER" Event with ',I4,' block;',/,
     *          ' Array sizes in ANALYZE can handle only',i3,' blocks')
        RETURN1
      END IF

      DO  J=1,NBLOCK
```

```
      IPOINT=KOUNT+8+14*(J-1)
C nscale is 6
      DO  I=1,NSCALE

        INT2(1)=IREC(IPOINT)
        INT2(2)=IREC(IPOINT+1)

        SCBUF(I,J)  =  INT4

        SCALER(I,J)=SCALER(I,J)+INT4

        IVAL  =  I+(J-1)*NSCALE

        IPOINT  =  IPOINT  +  2
      ENDDO
    ENDDO
    RETURN
    END
```

Appendix C

Detectors are made of NE102 plastic scintillator.

B1	⊘ 32 × 3.2 mm (⊘ 1.3" × 1/8")
B2	⊘ 32 × 3.2 mm (⊘ 1.3" × 1/8")
B3	⊘ 27 × 3.2 mm (⊘ 1.1" × 1/8")
S1	⊘ 203.2 × 1.6 mm (⊘ 8" × 1/16")
S2	⊘ 355.6 × 101.6 mm (⊘ 14" × 4")
S3	⊘ 365.8 × 12.7 mm (⊘ 14.4" × 1/2")
C	(outside dia.) ⊘ 203.2 × 340 × 3.2 mm (⊘ 8" × 13.4" × 1/8")

Table C.1 Detector sizes.

Appendix C. Detectors

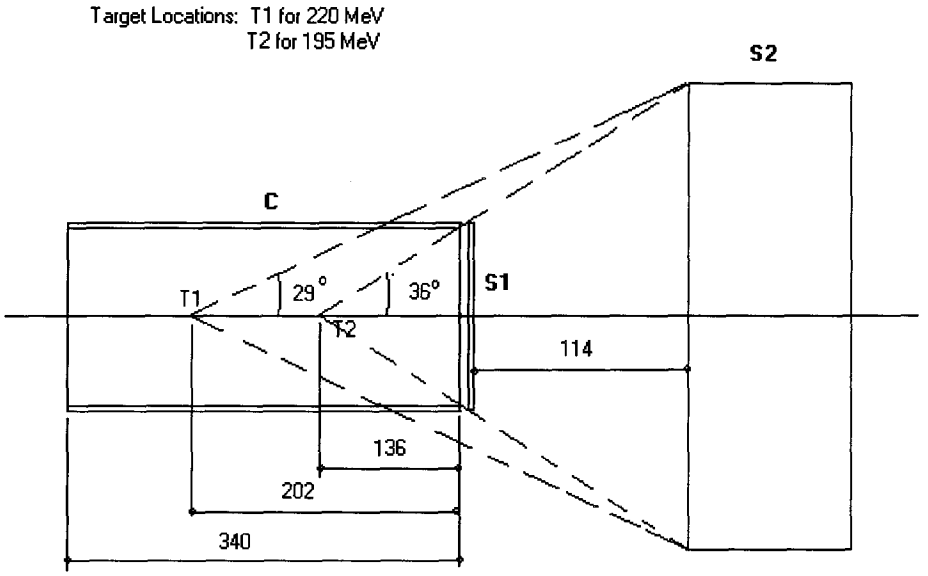

Figure C.1 Target geometry.

Appendix C. Detectors

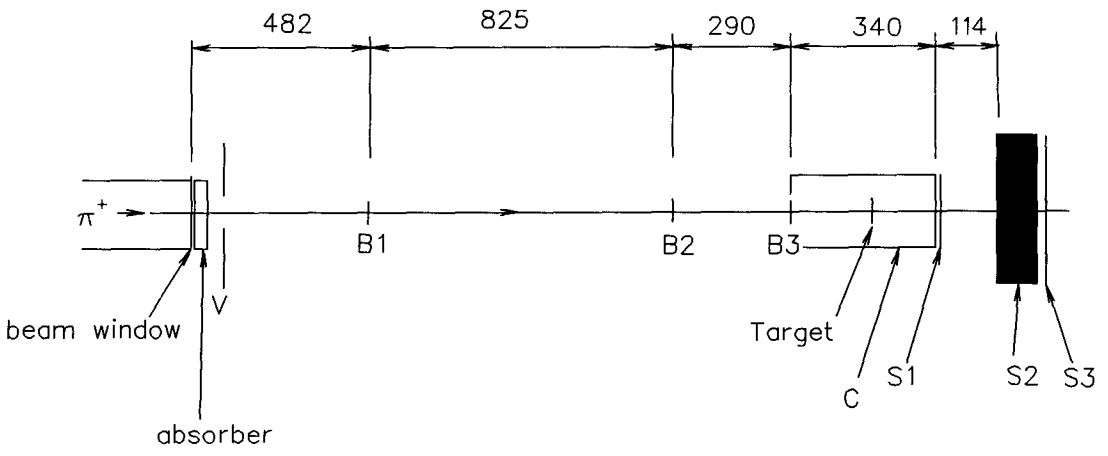

Figure C.2 Detector geometry.